ADVANCED OPTICAL MATERIALS
www.advopticalmat.de

Recent Advances in Block Copolymer Self-Assembly for the Fabrication of Photonic Films and Pigments

Zhen Wang, Chun Lam Clement Chan, Tianheng H. Zhao, Richard M. Parker, and Silvia Vignolini**

The self-assembly of block copolymers (BCPs) into photonic materials has drawn significant attention due to the flexibility and diversity of the building blocks that can be synthesized. This review provides a brief overview of the development of this research area and then discusses in detail recent advances in the use of BCPs as photonic pigments. In particular, the role of confinement upon the self-assembly process to form well-ordered lamellae is described and compared to correlated disordered structures derived from densely packed micelles. These systems respectively act as 1D (multilayered) photonic crystals and photonic glasses and are here critically compared in terms of their structural characteristics and optical performance. Finally, based on this understanding, the current challenges in this field are discussed and the potential for future developments is explored.

1. Introduction

Block copolymers (BCPs) are an interesting class of material that has been proven effective in fabricating photonic materials due to their capability to self-assemble into structures on the scale of the wavelength of visible light. When compared with other materials employed in bottom-up self-assembly (e.g., colloids), BCPs possess several advantages, such as rapid kinetics, macroscopic ordering of the self-assembled structures, and tolerance to a high loading of functional additives.[1–4] Moreover, the possibility to manipulate the produced coloration simply by tuning the molecular structure of the underlying BCPs allows for their directed-assembly into more complicated microstructures.[5,6] This enables the production of photonic pigments, with colors spanning the entire visible spectral range and with tunable optical appearance.

In this review, we first provide an overview of the photonic structures that can be formed from block copolymers via a self-assembly pathway. This is followed by the development history and recent progress of 1D photonic films, also commonly referred to as photonic multilayer structures. In the third section, recent advances in exploiting confined self-assembly of block copolymers to produce photonic pigments are introduced and the diversity of structures that can be achieved with this method explored, ranging from concentric lamellae to porous particles with correlated disorder. Finally, we conclude by highlighting promising directions for future investigation.

Z. Wang, C. L. C. Chan, T. H. Zhao, R. M. Parker, S. Vignolini
Yusuf Hamied Department of Chemistry
University of Cambridge
Lensfield Road, Cambridge CB2 1EW, UK
E-mail: rmp53@cam.ac.uk; sv319@cam.ac.uk

The ORCID identification number(s) for the author(s) of this article can be found under https://doi.org/10.1002/adom.202100519.

DOI: 10.1002/adom.202100519

2. Block Copolymer Self-Assembly for Photonic Structures

The self-assembly of block copolymers has been extensively used to prepare a large variety of photonic and plasmonic structures, including lamellae, hexagonally-packed cylinders,[7,8] closely-packed micelles,[9,10] double diamond,[11] gyroids,[12,13] correlated networks and cubic,[14,15] and photonic glasses.[8,16–18] Despite this wide variety, the most commonly reported architecture is by far based on the lamellar structure, as it is both simple to obtain and offers the best performance with respect to the optical response (i.e., maximal reflectivity from the smallest size). As such, this section focuses on the development of linear and brush block copolymers to produce lamellar structures, with emphasis placed upon the progress made within the past two years. For a summary of the early growth of the field, we recommend previous review papers on the topic.[5,6,19–21]

2.1. Development of 1D Photonic Structures from Block Copolymers

Linear block copolymers (LBCPs) are composed of two or more linear polymeric segments. When the segments possess distinct chemical properties and are of comparable volume, they can spontaneously undergo microphase-separation above a threshold concentration in specific solvents, to form a well-defined lamellar structure that can be retained into the solid-state.[2,6] Although a wide range of LBCPs have been reported to assemble into such lamellar structures, a photonic response is only produced when there is both sufficient difference in refractive index between the blocks, and the domain spacing of the lamellar structure is on the scale of the wavelengths of visible light.[22–24]

In his pioneering work in 1999,[25] Edwin Thomas first proposed the use of LBCPs as building blocks for photonic materials and presented methods that could be used to achieve structural color. In his following studies, this concept was realized using poly(styrene-*b*-ethylene/propylene) (PS-*b*-PE/P) with a large molecular weight (MW) of 400 kDa for each block.[26–28] This was shown to self-assemble into a 1D periodic lamellar structure with a domain spacing of around 200 nm, producing a colored reflection with peak reflectance wavelength (λ_{max}) at 545 nm.[26] Furthermore, by selectively loading different amounts of gold nanoparticles, the reflected light could be shifted to longer wavelengths.[28] After these initial demonstrations of structural color, Thomas and co-workers reported that this concept could be applied to a second polymer system, poly(styrene-*b*-isoprene) (PS-*b*-PI).[29,30] PS-*b*-PI with high MWs were synthesized using anionic polymerization with the sequential addition of styrene and isoprene monomers. By microphase separation of the PS and PI blocks, these LBCPs formed a lamellar morphology with the domain spacing correlating to the molecular weight. By varying the molecular weight, they were able to produce photonic films with a range of different colors (λ_{max} = 375–500 nm). A similar method to obtain structurally colored films was subsequently demonstrated by Sohn et al.[31] Since these early examples, many other LBCPs have been designed and synthesized for photonic films, including poly(methylenecyclopentane-co-3-vinyltetramethylene)-*b*-poly(ethylene-co-norbornene),[32] linear low density polyethylene-*b*-ultra low density polyethylene,[33] polystyrene-*b*-poly(solketal methacrylate),[34] and polyisoprene-*b*-poly(4-methylstyrene).[35] However, it should be noted that the synthesis of LBCPs with such large MWs is often challenging to achieve.

To provide an overview of the research in this field and to identify the evolution of the topics explored, a co-occurrence map for common keywords (derived from those appearing on the publications themselves) was produced using "VOSviewer." As shown in **Figure 1**a, each node represents a keyword describing a subtopic, with the size of the node proportional to the number of associated publications and its color indicating the average publication year for those papers. Lines connecting pairs of nodes indicate that at least one paper can be described by both of those keywords. Other than the main keywords of "block copolymer," "photonic crystal," and "self-assembly," which were ubiquitous amongst most of the works surveyed and as such disregarded, this map revealed that the most frequently investigated subtopics are "tunable color," "responsive," "solvent swelling," "gel," and "sensor." This demonstrates that the BCP community is primarily focused upon developing advanced functionalities, rather than continuing to explore the fundamental polymer chemistries used to build such photonic structures. In addition, several research directions, such as "inkjet printing," "confinement," "ionic liquid," "programmable patterning," and "photo-thermal writing," have recently emerged, suggesting that as the field matures, the focus is moving toward both applications and developing complex systems.

In order to highlight how the field has developed and evolved, the relative contributions of authors in this field have been identified using a co-author collaboration network, as shown in Figure 1b. This network additionally summarizes the authorship of papers on this topic, highlighting the links and collaborations between different authors. Each node represents a researcher (defined here as any author listed on a paper). The node size is proportional to the number of papers published by this researcher while its color represents the average publication year of those paper, similar to that in Figure 1a. Lines connecting two nodes indicate that the linked researchers have appeared together on at least one paper. It should be noted that not all researchers' names are shown explicitly in this figure, especially within denser regions. Some nodes group into a cluster representing a specific research interest in which these researchers are closely related. The research contribution and influence of Edwin Thomas to the development of the field over the last 22 years is markedly shown by the size of his node and associated collaborator network. In fact, with 43 papers, this network accounts for nearly fifty percent of all publications to date. Many of their works will be heavily featured in the following discussions on the development of LBCP-based photonic structures.

Beyond the photonics community, the most frequently and widely investigated LBCP is polystyrene-*block*-poly(2-vinyl pyridine) (PS-*b*-P2VP). However, due to the chains being limited to shorter lengths (M_W < 450 kDa) and the similar refractive indices between these two blocks (n_{PS} = 1.59; n_{P2VP} = 1.62), it is challenging to produce a structurally colored film directly from PS-*b*-P2VP. Instead, it is often necessary to dope the lamellar structures with additives. The first demonstration of this concept was presented in 2007,[38] whereby the domain spacing, which was originally 100 nm, was increased, up to 640 nm, by quaternizing the pyridine groups and controllably swelling the quaternized P2VP (QP2VP) domains with an aqueous salt solution (**Figure 2**). This increase in domain size, coupled with the accompanying reduction in refractive index, led to a tunable reflection spanning from the ultraviolet to the near infrared. By unlocking a pathway to fabricate photonic films from LBCPs that do not possess large molecular weights, this approach has now been extensively emulated to fabricate a wide range of stimuli-responsive PS-*b*-P2VP photonic films. Examples of stimuli used to tune the optical response have included pH,[39–41] electric field,[42–48] solvents,[49–67] pressure,[68] and temperature.[69] In addition, by blending nanoparticles into the domains of the lamellar structures, the reflected color can also be tuned.[70] The resulting "smart" materials can be employed for a range of applications, such as chemical sensing,[56,71,72] mechanical sensing,[68,73] biological sensing,[74,75] and displays.[44,48,76]

Supramolecular complexation has also been reported as a viable strategy to expand the dimensions of LBCPs and correspondingly shift the optical response into the visible spectrum. Although polystyrene-*block*-poly(4-vinylpyridine) (PS-*b*-P4VP) possesses similar chemical properties to PS-*b*-P2VP, the accessibility of the nitrogen site allows for the introduction of guest molecules that can complex with the pyridine group.[77,78] In these studies, dodecylbenzenesulfonic acid (DBSA) and 3-*n*-pentadecylphenol (PDP) were used as guest molecules to interact with the pyridine group within PS-*b*-P4VP via electrostatic interactions or hydrogen bonding, which significantly expands the thickness of the lamellae. As a result, despite the native PS-*b*-P4VP not reflecting visible light, the complexed system demonstrated a strong reflection in the visible spectrum. However, at higher temperatures dissociation of the

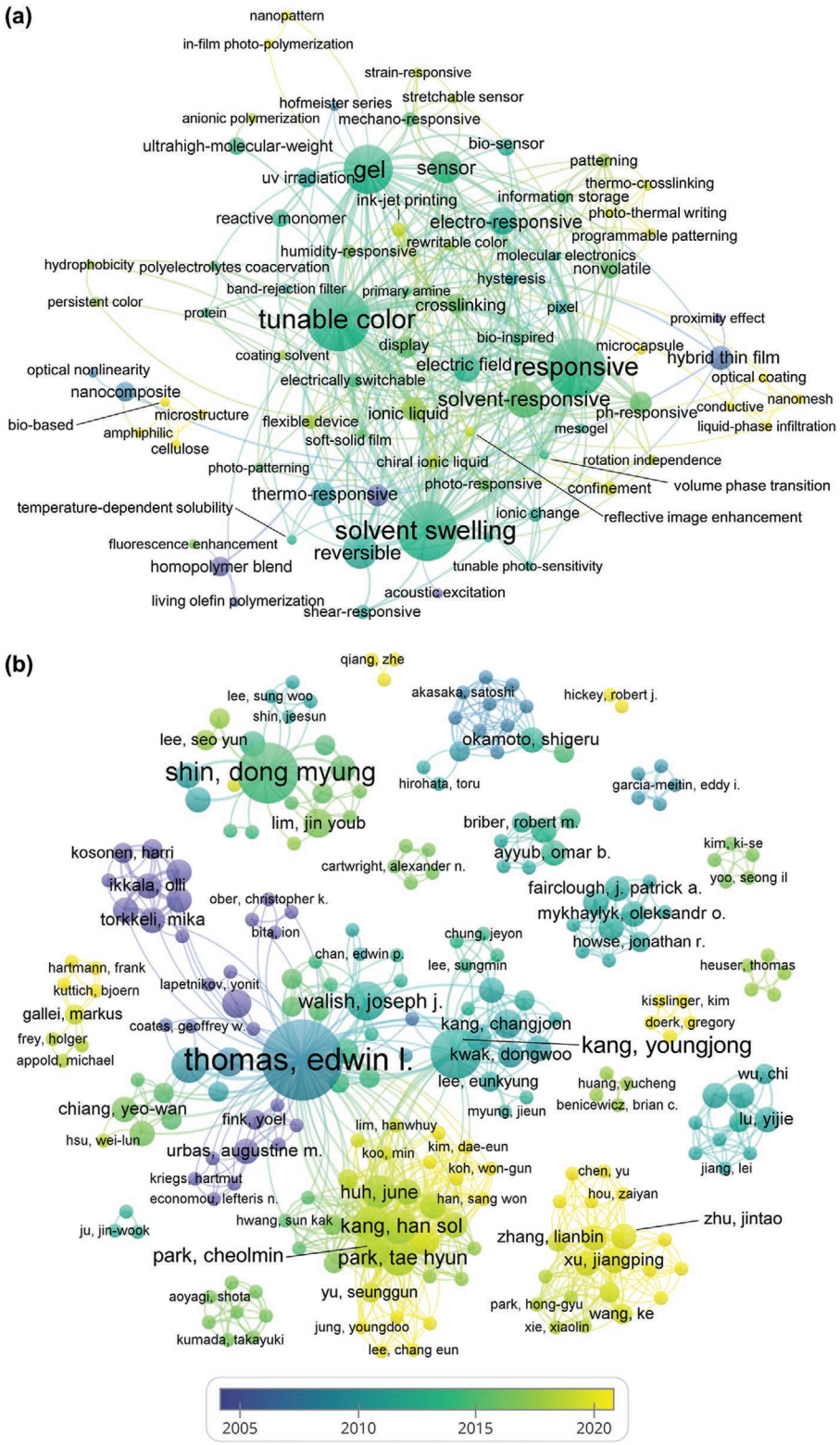

Figure 1. a) A keyword co-occurrence map and b) the corresponding co-author collaboration network for research investigating the application of linear block copolymers for photonic films or pigments. In (a), each node highlights a subtopic, with relationships indicated by the linkages, while in (b) each node represents a contributor to this field, with collaborations indicated by the linkages such that clustering indicates a common research theme. Due to the limited space, not all researcher names could be labeled. The size of each node is proportional to the number of publications and the color represents the average publication year. The keywords in (a) are derived from those appearing on the publication or where absent, extrapolated from the abstract, introduction, or conclusion of the article. The figure was obtained using VOSviewer.[36,37]

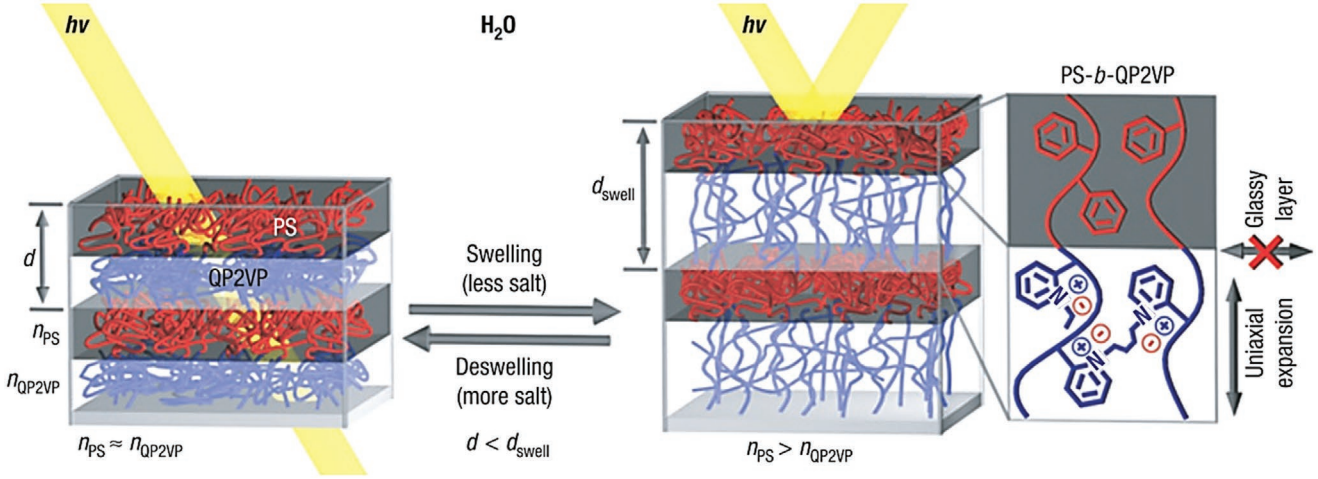

Figure 2. Schematic illustration of the controllable swelling of a PS-*b*-QP2VP lamellar structure into a photonic gel using salt. By selectively swelling the QP2VP block, both the domain spacing (d) and the refractive index contrast ($\Delta n = n_{PS} - n_{QP2VP}$) of the multilayered photonic crystal increase, allowing for reflection of visible light. Reproduced with permission.[38] Copyright 2007, Springer Nature.

hydrogen bonds was observed, resulting in the complexes becoming unstable and leading to a reduction in the domain spacing with a corresponding loss of color.

These strategies can also be applied to other LBCP systems, with the optical response of PS-*b*-PI films often tuned from an initial colorless state to visible wavelengths via solvent swelling[79–87] or the incorporation of PS or PI homopolymer into the domains.[83,88,89] Similarly, photonic films based upon polystyrene-*b*-poly(methacrylic acid),[90] polystyrene-*b*-polymethacrylate,[91] polystyrene-*b*-poly(*tert*-butyl methacrylate),[92,93] poly(3-(triethoxysilyl)propyl methacrylate)-*b*-poly(stearyl methacrylate)[94] have also been successfully prepared and tuned via supramolecular chemistry, doping with nanoparticles, or solvent swelling.

Although a wide variety of LBCPs have been exploited to produce photonic materials, they share some intrinsic disadvantages: i) The long polymer chains cannot be easily synthesized based on current polymerization techniques, with such polymers typically requiring a high degree of polymerization. This can result in slow and uneven chain propagation that can hinder the ability to obtain monodisperse long polymer chains. ii) The complex molecular topology and conformation of LBCPs in solvent can cause slow self-assembly dynamics.[5,6,95,96] An alternative class of BCP, the brush block copolymer (BBCP), also known as a bottlebrush block copolymer or molecular brush, promises to alleviate these issues, allowing for greater access to photonic materials. BBCPs have densely grafted side chains and the strong steric hindrance of these side chains significantly increases the rigidity of the polymer backbone, which extends the conformation of the BBCP and reduces chain entanglement. In turn, these lead to large and well-defined molecular dimensions and rapid self-assembly kinetics.

The first example to demonstrate the ability of BBCPs to self-assemble into photonic films was reported by Rzayev.[97] Poly(polystyrene)-*b*-poly(polylactide) P(PS)-*b*-P(PLA) was synthesized via a combination of reversible addition–fragmentation chain-transfer (RAFT), atom transfer radical polymerization (ATRP), and ring-opening polymerization (ROP). A blue coloration was shown by a P(PS)-*b*-P(PLA) with a large MW (2.4 MDa) and densely grafted side chains. However, few further studies were reported to use this method to produce structural coloration, potentially because of the inconvenience of synthesizing BBCPs by this grafting-from route. Nevertheless, the subsequent development of Grubbs catalysts unlocked a facile synthetic route toward BBCPs using a grafting-through approach, and therefore promoted the feasibility of BBCPs for photonic materials and applications.

In a seminal paper published in 2009, Grubbs et al. first demonstrated that a BBCP synthesized using a Grubbs catalyst could be self-assembled into photonic films.[98] In this paper, the authors synthesized norbornenyl poly(*n*-butyl acrylate) (I-P*n*BA) as the first macromonomer (MM, a polymer or oligomer with a polymerizable bond) and norbornenyl polylactide (I-PLA) as the second MM. With sequential addition of two MMs, a BBCP was polymerized via ring-opening metathesis polymerization (ROMP) as poly(I-P*n*BA)$_{200}$-*b*-poly(I-PLA)$_{200}$ with an identical degree of polymerization (DP) of 200 for both blocks. A green structurally colored film was produced by slowly evaporating a solution of the BBCP (**Figure 3**b). The authors proposed that the ultrahigh-molecular-weight BBCPs self-assembled into a lamellar structure with a domain spacing large enough to reflect in the green spectral region. This new synthetic pathway has been widely taken up by the community, with almost all BBCP-based photonic films reported since synthesized by applying ROMP to copolymerize two norbornenyl-based MMs. By varying the different side chains of the MMs employed, a diverse library of photonic BBCPs has been constructed, with notable examples including: wedge-type side groups,[99–101] isocyanate-based side chains,[102,103] polystyrene,[104,105] poly(*tert*-butyl acrylate),[106] polyethylene oxide,[107–109] poly(benzyl methacrylate),[110] and silsesquioxane pendants.[110]

The ability to precisely control the polymerization of MMs has enabled BBCPs with MWs of up to 7 MDa (M_n) to be successfully synthesized, well beyond the limit achievable by their linear analogs.[111] In addition, these polymers are very

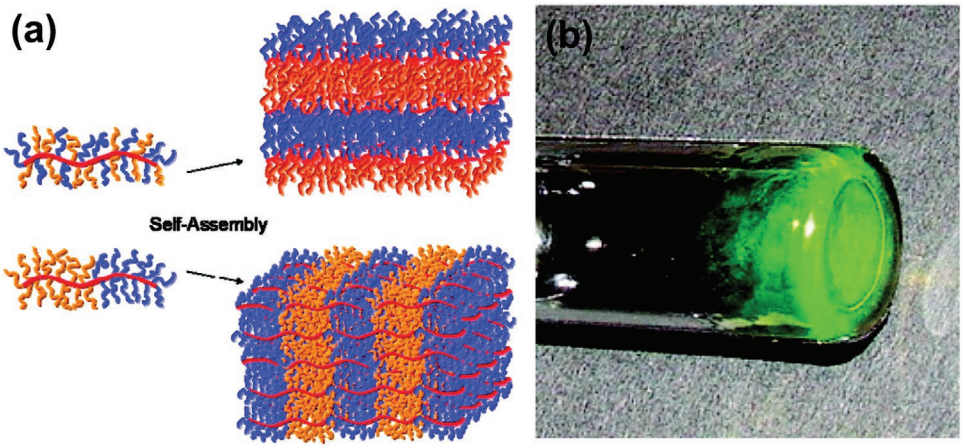

Figure 3. a) Self-assembly of brush random copolymer and block copolymer. b) Optical image of a slowly dried poly(I-P*n*BA)$_{200}$-*b*-poly(I-PLA)$_{200}$ sample, showing vivid green color. Reproduced with permission.[98] Copyright 2009, American Chemical Society.

well-defined with the polydispersity indices (PDI) typically under 1.3. As a result, reflections at long wavelengths can be achieved, reaching the near-infrared range without any additives,[99,101–104,107,110] and up to 1400 nm by blending in homopolymers.[105] Finally, this combination of ultrahigh MW, narrow PDI, and predictable rod-like conformation in solvent, results in a linear relationship between MW and λ_{max}, allowing for the rational design of BBCP-based photonic films with a specific optical response.

Similar to that observed for linear BCPs in Figure 1a, the terms "tunable color," "responsive," "solvent swelling," and "dendronized macromonomer" have all been hot topics in the photonic BBCP community (**Figure 4**a). However recent research has shown a growing interest in producing photonic pigments with new nanoarchitectures, as indicated by the appearance of "confinement," "photonic pigment," "microsphere," "non-iridescent," and "inverse photonic glass." Figure 4b reports the analogous co-author collaboration network for BBCP-based photonic materials. Given the development of this area was accelerated with the discovery of the Grubbs catalyst, it is not surprising to see that Robert Grubbs, Garret Miyake, Raymond Weitekamp, and Jae-Suk Lee hold a prominent role, together accounting for 38% of all articles published on this topic. Linked to them, Dylan Walsh and Damien Guironnet have recently started to be involved in similar topics. A separate cluster has developed, as visualized across the top left side of Figure 4b, indicating that several other researchers have begun to investigate this research topic. In particular, Dong-Po Song has been contributing to the preparation of a variety of novel photonic structures.

2.2. Latest Advances in Block Copolymer-Based Photonic Films

2.2.1. Linear Block Copolymers

Although the most frequently used LBCP remains PS-*b*-P2VP, over the past two years there has been little progress towards increasing the molecular weight of the blocks so that visible color can be reflected from the lamellar structure in the absence of dopants. Instead, most of the recent publications have adopted swelling as a method to shift a colorless PS-*b*-P2VP film into the visible regime, as previously introduced in Section 2.2 and Figure 2. In particular, nonvolatile solvents, such as ionic liquids, have been explored as ideal swelling agents, as this avoids the issue of the loss of structural color upon solvent evaporation.[63,65] The inclusion of ionic liquids has the additional advantage of allowing the domain spacing (and correspondingly the color of the photonic film) to be tuned with magnetic or electric fields.[112]

Park et al. reported printable and rewritable structurally colored films for use in a humidity sensor by combining PS-*b*-QP2VP with different ionic liquids (**Figure 5**).[113] This was achieved by selectively infusing poly(ethylene glycol diacetate) (PEGDA) oligomers and a photoinitiator into the QP2VP domains. After exposure to UV light, a robust solid-state photonic film incorporating an interpenetrated hydrogel network (IHN) was formed. The amount of IHN was controlled through the loading of PEGDA and the UV irradiation time. With different degrees of crosslinking, the thickness of the P2VP layer was tuned from 105 to 158 nm, corresponding to domain spacings from 150 to 203 nm (as the PS domain remains constant at 45 nm), enabling reflection across the full visible wavelength range. When the films were swollen by the ionic liquid, 1-ethyl-3-methylimidazolium bis-(trifluoromethylsulfonyl)-imide (EMIM-TFSI), the structural color was redshifted from the initial λ_{max} at 570 nm (set by controlling the crosslinking degree) to over 1000 nm with increasing amounts of EMIM-TFSI. Interestingly, they were able to use the photonic film as a substrate for ink-jet-printed structurally colored patterns, which could be erased and rewritten multiple times by removing and adding again the ionic liquid ink (Figure 5b). Finally, when a hygroscopic ionic liquid, such as lithium bis-(trifluoromethanesulfonyl)-imide (Li-TFSI) ink was used, the color of the structurally colored surface became responsive to environmental humidity, with sensitivity such that the localized humidity of a human finger could induce a color change (Figure 5c). However, it is important to note that the first demonstration of a LBCP for printable and rewritable structural color was first explored in 2017,[76] using ammonium persulfate

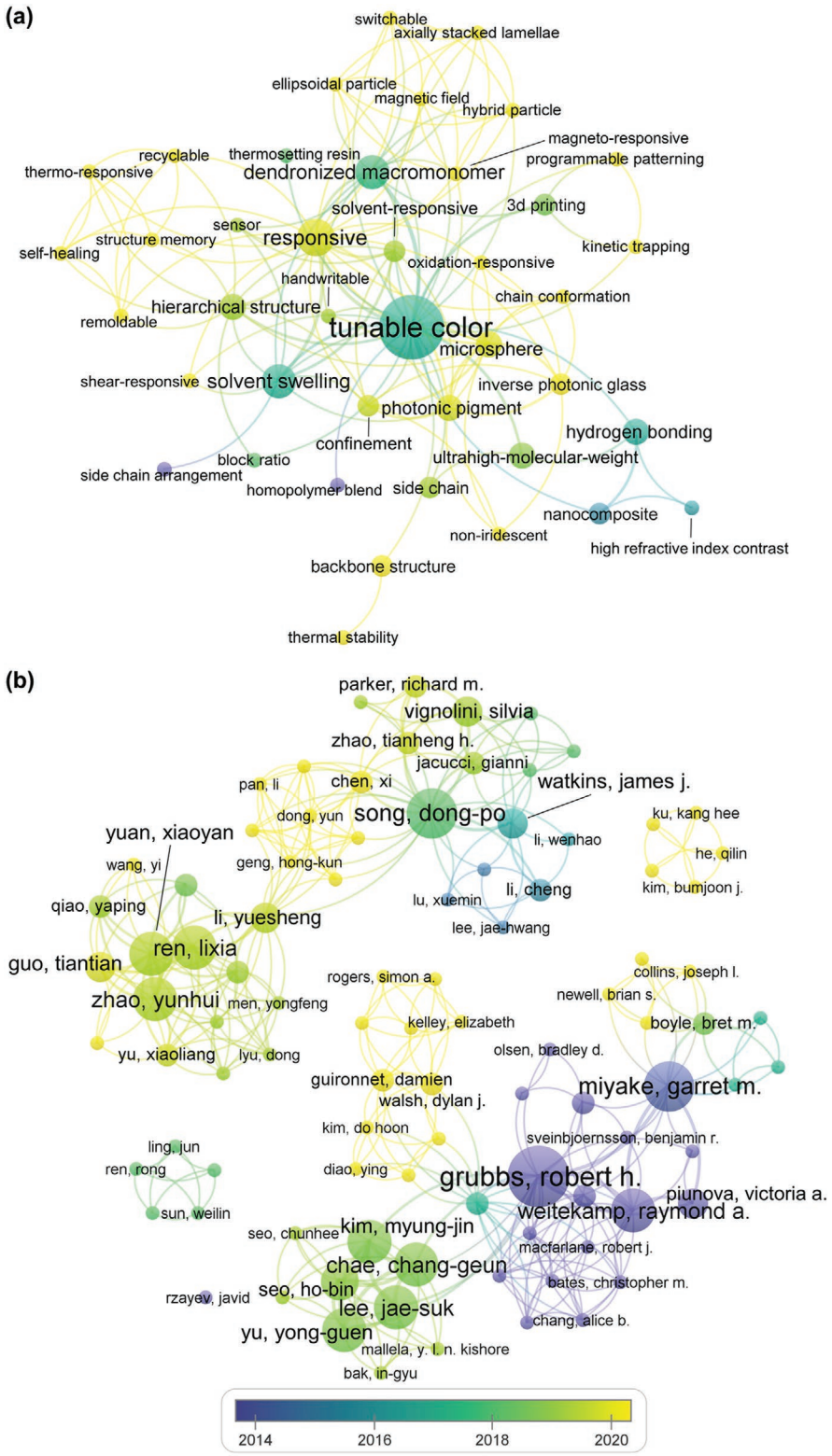

Figure 4. a) A keyword co-occurrence map and b) the corresponding co-author collaboration network for the field of brush block copolymer-based photonic films and pigments. In (a), each node highlights a subtopic, with relationships indicated by the linkages, while in (b) each node represents a contributor to this field, with collaborations indicated by the linkages such that clustering indicates a common research theme. Due to the limited space, not all researcher names could be labeled. The size of each node is proportional to the number of publications and the color represents the average publication year. The keywords in (a) are derived from those appearing on the publication or where absent, extrapolated from the abstract, introduction, or conclusion of the article. The figure was obtained using VOSviewer.[36,37]

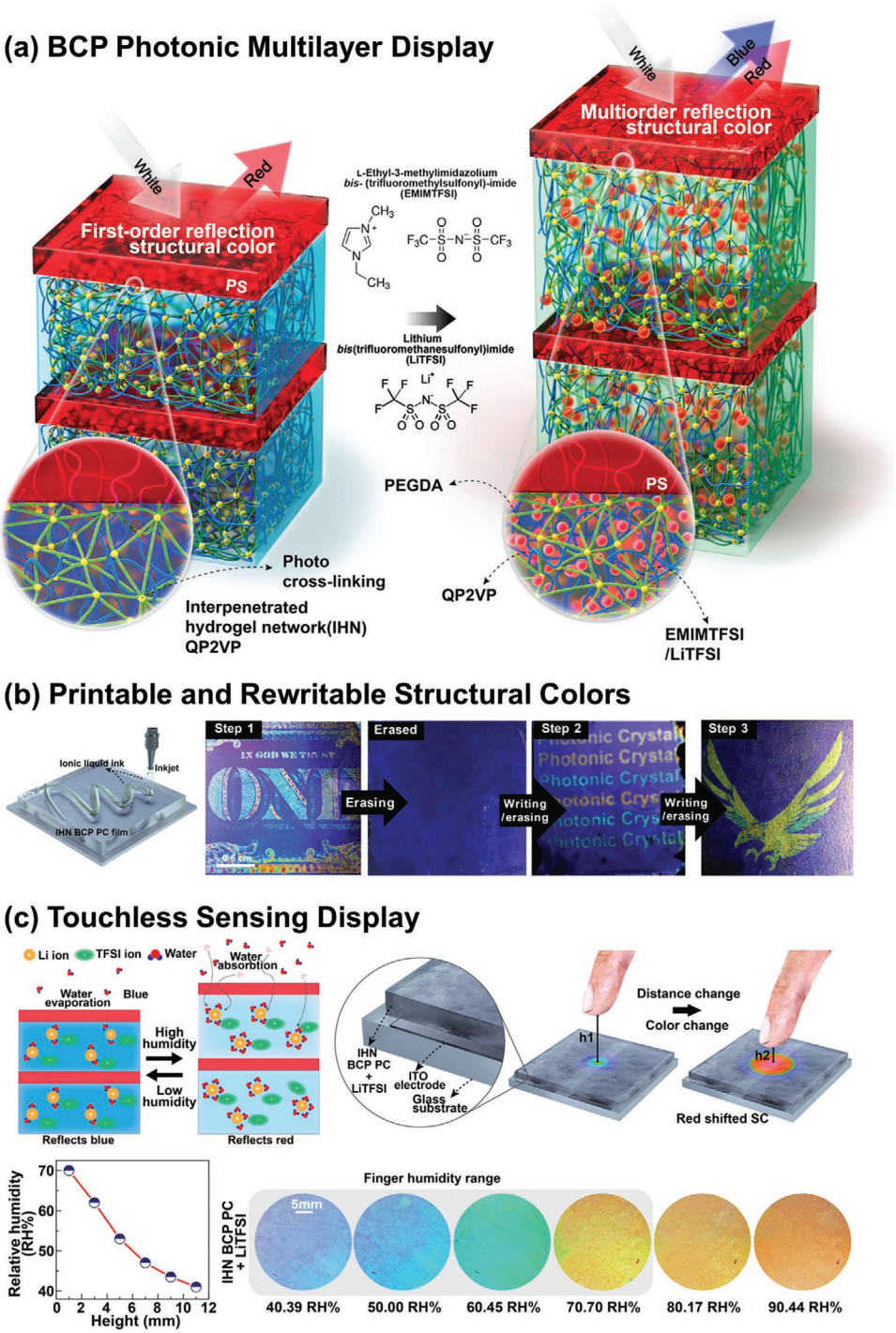

Figure 5. Examples of printable and rewritable block copolymer structural colors and a humidity sensing display based on PS-*b*-P2VP photonic films upon doping with different ionic liquids: EMIM-TFSI/Li-TFSI. a) Schematic illustrating the multiordered structural color arising from the swelling of the interpenetrated hydrogen network. b) Ink-jet printing of an ionic liquid, and its subsequent removal, can allow for rewritable structurally colored images. c) Changes in the local relative humidity can induce a color change in the BCP film allowing for a touchless sensing display to be produced. Adapted with permission.[113] Copyright 2020, The Authors, some rights reserved; exclusive licensee AAAS. Distributed under a Creative Commons Attribution NonCommercial License 4.0 (CC BY-NC).

and hydrogen bromide either to crosslink or to de-crosslink the QP2VP layer. When these two papers are compared in terms of mechanism, we believe that the physical diffusion method reported more recently[113] provides a better response than the chemical approach,[76] which may cause accumulation of ions leading to a reduction in responsivity.

Compared to the example shown above, where manual addition and removal of the ionic liquid are required to refresh the

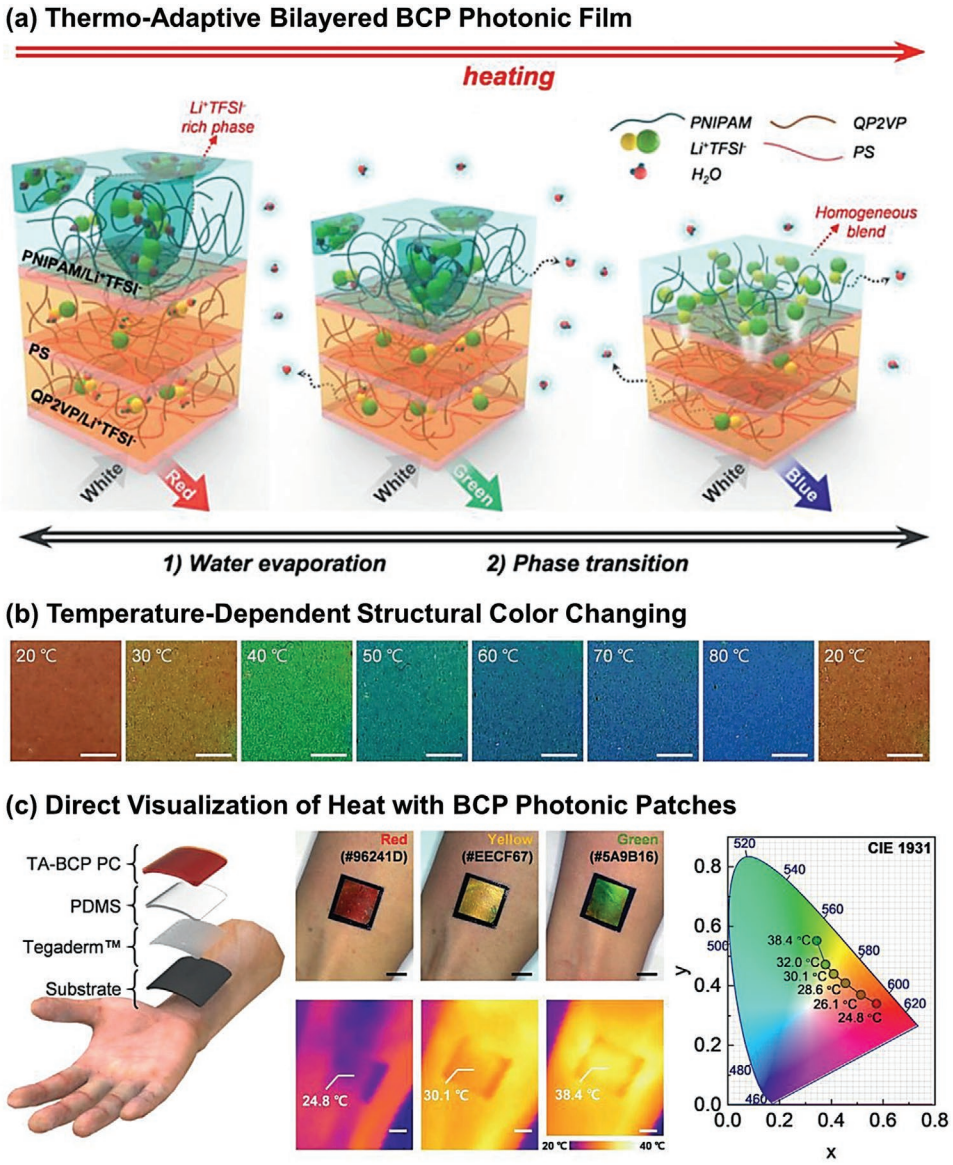

Figure 6. Example of a thermoadaptive block copolymer photonic composite film, highlighting the temperature-dependent structural color and its potential application as flexible patches in thermo-sensing scenarios. a) Schematic illustrating the origin of the structural color change upon heating the bilayered BCP photonic film. b) Photographs showing the temperature-dependent structural color change. Scale bar is 3 mm. c) Schematic of the BCP photonic patches used as thermochromic sensors (left). Photographs and corresponding IR thermal images of the patches on a wrist (center). Scale bar is 1 cm. CIE coordinates of the patches as a function of temperature (right). Adapted with permission.[114] Copyright 2021, Wiley-VCH.

display, a self-adaptive system would be a more efficient method to control the structural color of the film. Yu et al. constructed a thermoadaptive structural colored system as flexible patches for thermo-sensing scenarios.[114] A poly(*N*-isopropylacrylamide) (PNIPAM) and Li-TFSI blend solution was spun-coated onto a PS-*b*-QP2VP photonic film. The QP2VP domain was partially swollen with water and Li-TFSI, endowing the photonic device with a thermochromic optical response. When the temperature increased from 25 to 80 °C, the water in the P2VP domains evaporated. In addition, at temperatures above the sol-gel transition point of the PNIPAM/LI-TFSI mixture, which is approximately 40 °C, the Li-TFSI migrates from P2VP domain into the PNIPAM layer. Combined, these two effects decreased the degree of swelling of the QP2VP domains, leading to a contraction of the domain spacing of the multilayered structure with temperature (**Figure 6**a). As a result, a blueshift of the structural color through the full visible spectrum was observed with an increase in temperature (Figure 6b). When the composite film was cooled back to room temperature, the optical response returned to the original wavelength. The authors exploited this effect to construct a heat detection patch for non-invasive visualization of the temperature of the human body (Figure 6c). A similar thermochromic response was developed by Thomas et al. in 2012, where structurally colored gels were prepared by swelling unquaternized PS-*b*-P2VP films with aqueous acetic acid solutions.[69]

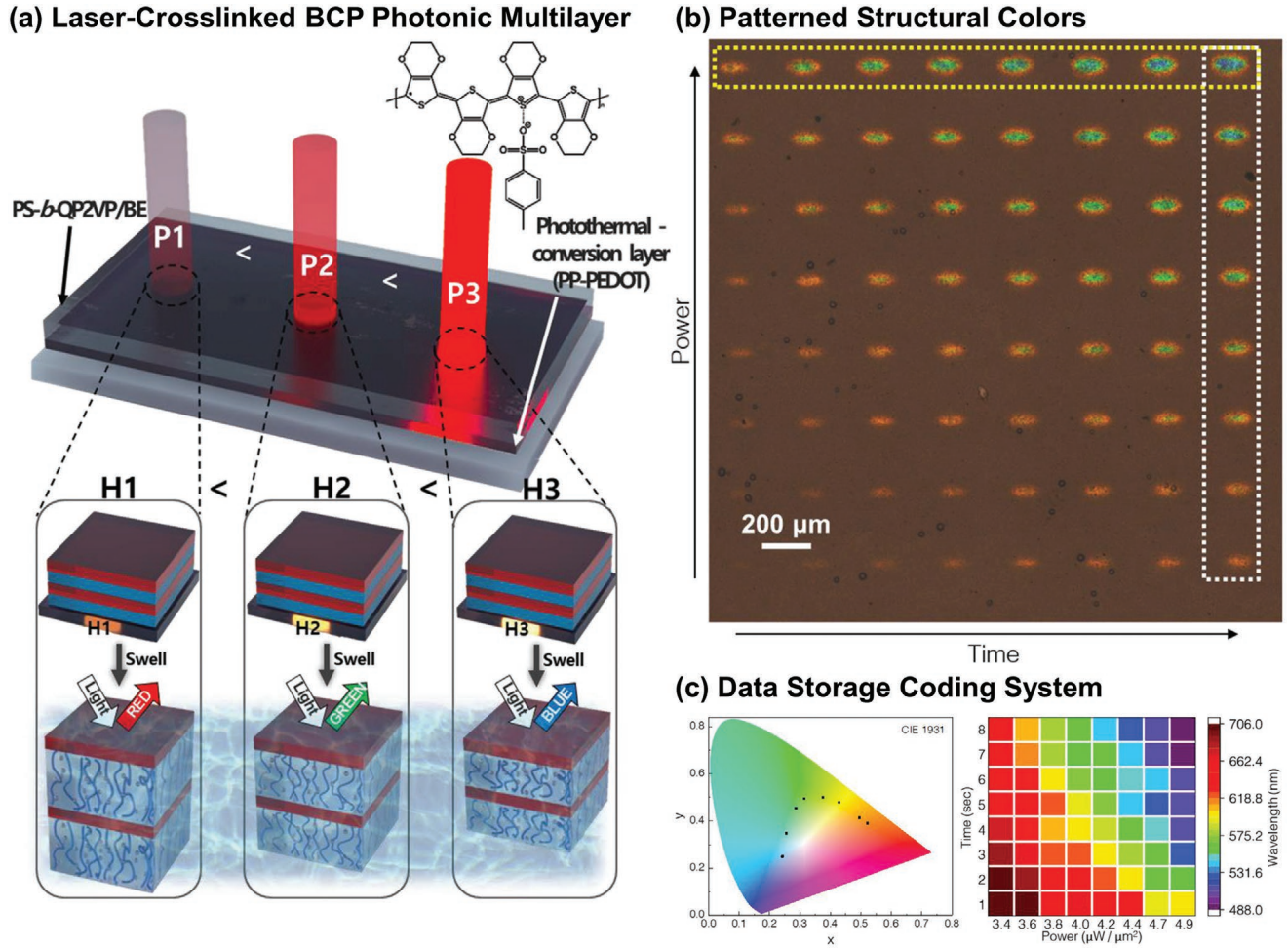

Figure 7. Example of photothermal writing of block copolymer structural color for data storage. a) Schematic showing that crosslinking via near-infrared laser irradiation, with the laser power correlated to the structural color. b) Optical microscopy images of the photothermally programmed structural colored film immersed in ethanol. c) CIE coordinates and the color window of the patterned structural color in image (b). Adapted with permission.[115] Copyright 2019, Wiley-VCH.

Recently, Kang et al. found that radicals can be generated in QP2VP domains by heating, which can directly crosslink the QP2VP polymer chains.[115] By varying the amounts of quaternization and crosslinking agents used, different degrees of crosslinking were achieved across a range of temperatures. To induce crosslinking in more precise and localized areas, heating was realized via photothermal conversion using poly(3,4-ethyl-enedioxythiophene) doped with tosylate (PP-PEDOT) (**Figure 7**a). With programmed laser power and irradiation time, a PP-PEDOT layer converted light into different amounts of thermal energy, which was then transferred to the PS-*b*-P2VP photonic film. A 2D array of structural colors was created to demonstrate the potential of using photothermal structural color as bits in information storage (Figure 7b,c). As a showcase, the word "ONLY" was written and stored in combinations of four structural colors. As such, temperature, either applied directly or through a photothermal response, is a promising stimulus to tune the structural color of BBCP films as it can be applied remotely.

Beyond developing new methods to tune PS-*b*-P2VP, such as applying vapor- or liquid-phase infiltration,[116,117] recent studies have also explored more novel LBCPs and their application in photonic materials. A notable example is polystyrene-*block*-poly(2-hydroxyethyl methacrylate) (PS-*b*-PHEMA) by Gallei and co-workers.[118] In this work, PS_{72}-*b*-$PHEMA_{28}$[201] (M_n = 201 kDa, volume fraction of PHEMA is 28%), was used resulting in spherical micelles without any color. When cellulose fibers were blended into this polymer, a lamellar structure was formed. Depending on the amount of cellulose added, the reflected color could be adjusted from violet to blue. This work showcased the possibility of using natural polymers to tune the structure of block copolymer aggregates and render them into photonic materials. Another polymer system exploited to produce a photonic response is poly(1,2-butadiene)-*block*-poly(ethylene oxide) (1,2PBD-PEO). Xu and Hickey prepared this polymer with M_n of 66.1 kDa and PEO volume fraction of 43 via living anionic polymerization (LAP).[119] When the polymer was solution-cast on substrate and thermally annealed, a lamellar structure was formed. Due to the limited domain spacing (78 nm), blue structural color was achieved by selectively swelling a single block, either by adding hexane to the 1,2PBD block or water to the PEO block, while a green color

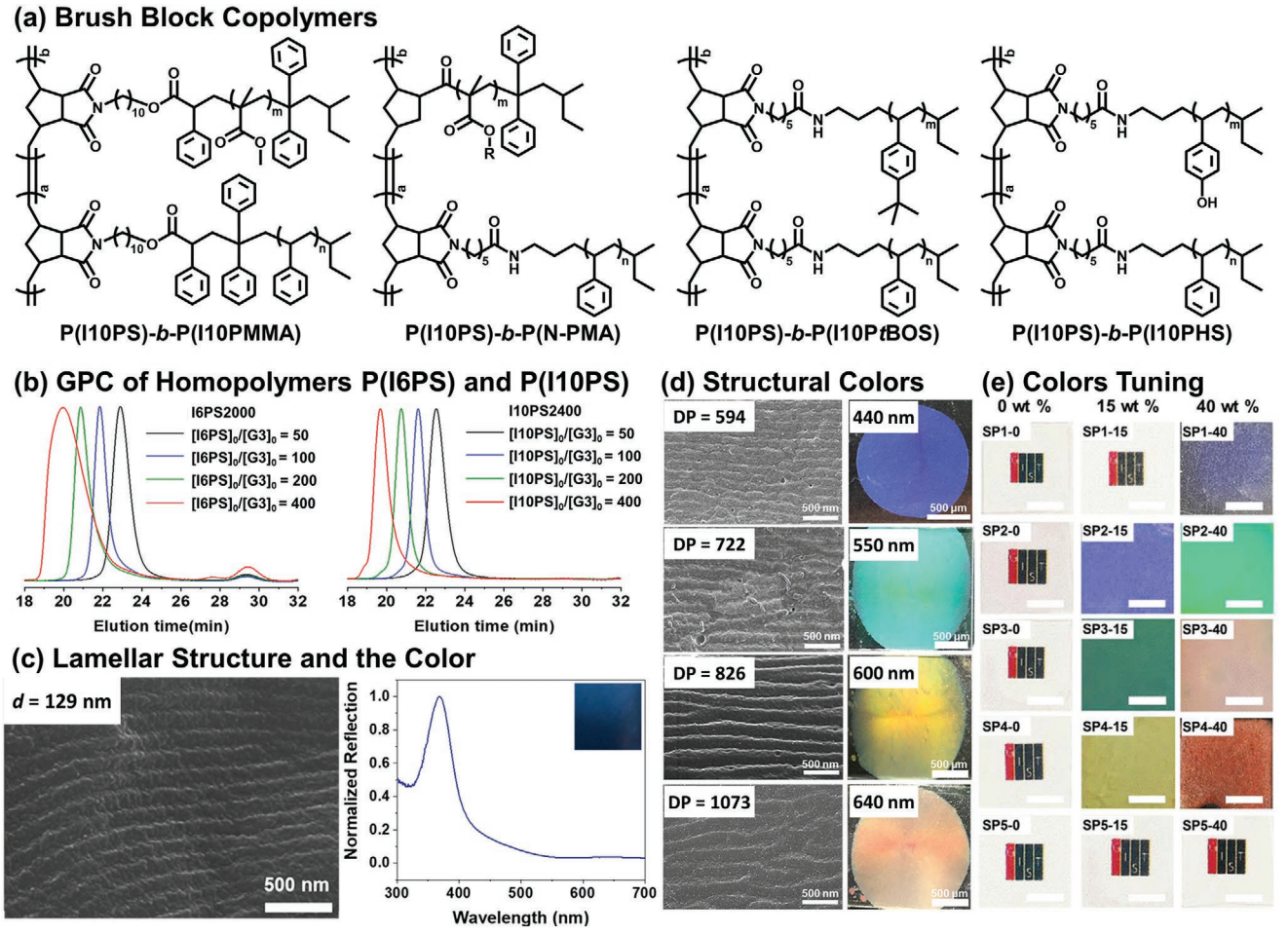

Figure 8. a) Examples of four types of brush block copolymers with a spacer between the norbornene unit and the side chain. b) Gel permeation chromatography (GPC) curves of homopolymers, P(I6PS) and P(I10PS). Adapted with permission.[120] Copyright 2019, American Chemical Society. c) Lamellar structures and structural colors of $P(I10PS)_{300}$-*b*-$P(I10PMMA)_{300}$. Adapted with permission.[120] Copyright 2019, American Chemical Society, and d) P(I10PS)-*b*-P(I10P*t*BOS). Adapted with permission.[122] Copyright 2018, American Chemical Society. e) Tuning of the structural color of P(I10PS)-*b*-P(I10PHS) by blending with mPEG. Reproduced with permission.[123] Copyright 2019, American Chemical Society.

could be achieved by swelling both blocks using toluene or tetrahydrofuran.

2.2.2. Brush Block Copolymers

Compared to LBCPs, the BBCPs used to produce photonic structures in the past two years were more diverse in terms of composition, with the main parameter reported to tune the structural color typically the degree of polymerization (DP) of the backbone. This is because of the relatively large size of these macromolecules and a low dependence on ultrahigh DP to achieve lamellar structures of sufficient domain size to produce structural coloration. While all BBCPs reported were obtained by ROMP, the synthetic methods and compositions of the MMs differed. Lee et al. developed a novel norbornenyl-based MM with active end-capping agent for LAP and variable alkyl spacers.[120] Based on this norbornenyl moiety, a series of well-defined ω-norbornenyl polystyrene (IxPS) and poly(methyl methacrylate) (IxPMMA) MMs were synthesized (where x represents an alkyl spacer), as described in **Figure 8**a. The alkyl spacers allow for the steric hindrance between adjacent side chains to be decreased when polymerizing these MMs via ROMP, with a longer spacer giving rise to a more controlled polymerization in terms of lower PDI and high monomer conversion (Figure 8b). However, in this system, structural color was only observed for the BBCP films with the highest molecular weight, with $P(I10PS)_{300}$-*b*-$P(I10PMMA)_{300}$ reflecting an indigo color (Figure 8c). A large domain spacing should be expected for these DPs given the poly(norbornene) repeating unit is calculated to contribute 0.62 nm in length.[121] However, in this case, while reducing the steric hindrance of the side chains decreased the synthetic challenge, it also reduced the rigidity of backbone of the BBCPs, meaning that the incremental change to the domain spacing with increasing DP is lower than expected and thus less effective to reach the length scales required for a photonic response.

The Lee group also reported a series of BBCPs, composed of ω-end norbornenyl polystyrene (I10PS) MM as the first block and N-P*t*BMA (norbornene-poly(*tert*-butyl methacrylate))

or N-PMMA (norbornene-poly(methyl methacrylate)) MMs as the second block.[124] More than ten BBCPs of different molecular weights were obtained via ROMP while retaining the same ratio between the two blocks. When the total DP of these polymers was increased from 500 to 1000, the domain size of the resulting lamellar structures grew from 110 to 256 nm for P(I10PS)-*b*-P(N-P*t*BMA), corresponding to reflected wavelengths in the range 387 to 690 nm. While for P(I10PS)-*b*-P(N-PMMA), the reflected wavelengths redshifted from 479 to 556 nm with an increase in the polymer size from a DP of 600 to 1000. A similar polymerization strategy was also used to synthesize poly(norbornene imide-polystyrene)-*b*-poly(norbornene imide-poly(4-*tert*-butoxystyrene)) (P(I10PS)-*b*-P(I10P*t*BOS)) (Figure 8d), with lamellar structures obtained by heating under compression.[122] By changing the DP from 104 to 1073, photonic multilayers with domain sizes from 40 to 200 nm were achieved, allowing for a series of structural colored films to be prepared with colors ranging from blue to red (440–640 nm) for DP from 594 to 1073 (Figure 8d). The *tert*-butyl group in P(I10PS)-*b*-P(I10P*t*BOS) can be deprotected under acidic conditions, leading to polyhydroxystyrene (PHS) instead of P*t*BOS (Figure 8a).[123] Solution cast films of BBCP P(I10PS)-*b*-P(I10PHS) with DPs from 488 to 822 were found to form disordered structures when annealed at room temperature, however, annealing at higher temperature resulted in well-ordered lamellae with domain sizes between 67 and 114 nm. As these domain sizes are not sufficiently large to reflect visible color, poly(ethylene glycol) methyl ether (mPEG) was introduced as an additive to swell the PHS domains, by exploiting the hydrogen bonding interaction between hydroxystyrene and PEG. As a result, structural color across the full visible range, from blue (429 nm) to red (680 nm) could be achieved with different mPEG concentrations (Figure 8e).

The existence of a spacer unit in the MM has a significant influence on both the polymerization of the MM and the self-assembly of the resultant BBCPs. In order to have BBCPs with well-defined molecular weights, norbornenyl moieties with longer spacers are preferred as the decreased steric hindrance benefits the propagation of the polymer chain during the polymerization. However, more flexible side chains soften the main chain backbone, which disrupts the linear and efficient increase in domain spacing with an increase of DP. Conversely, having short spacers and long polymer side chain allows for a faster increase in domain spacing as a function of DP, but reduces the accessibility of large backbone DP, which may limit structural color to shorter wavelengths. This apparent contradiction poses a dilemma for the design of the perfect BBCPs for photonic multilayer films. Some strategies have been proposed to address this issue. Li et al. developed a semicrystalline BBCP containing PEO. The BBCPs were synthesized via ROMP using N-P*n*BA and N-PEO as MMs and without spacers. When these BBCPs were thermally annealed, hierarchical lamellar structures were formed. These structures had two levels of ordering: there is a microphase separated lamellar structure with layers comprising respectively of P*n*BA and PEO, while within the PEO layers, PEO crystallizes to form a second-order lamellar structure (**Figure 9**a). BBCPs with main chain DP from 350 to 550 gave rise to domain sizes from 156 to 242 nm at 80 °C. Due to the lack of spacers, the domain sizes were relatively

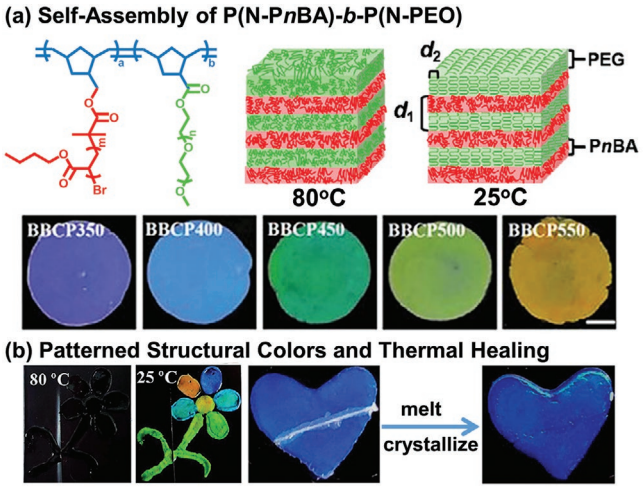

Figure 9. a) The self-assembly of P(N-P*n*BA)-*b*-P(N-PEO) into lamellar structures that display structural color, by exploiting crystallization of the PEO domains. b) Examples of patterned structural colored films and their temperature responsiveness and thermal healing property. Adapted with permission.[125] Copyright 2020, American Chemical Society.

large for the given DP and further increased by 7–10 nm when the temperature decreased to room temperature because of the crystallization of PEO. More significantly, as the refractive index of poly(N-PEO) increases from 1.46 to 1.64 upon crystallization, cooling to room temperature also increased the refractive index contrast between the two blocks that resulted in the appearance of bright color from the originally colorless films (Figure 9a). As this crystallization is reversible, the photonic multilayer structure can be switched between transparent and colored by simply melting and recrystallizing over several minutes. In addition, such materials can be shaped into complex patterns and are re-usable in the molten state (Figure 9b). As such, this study highlights an alternative strategy to the current design principles of BBCP.

BBCPs with dendronized wedge-like side chains have recently attracted attention as an alternative approach to address the balance between large domain spacing and polymerization control.[99] An AB_3-type unit in which three branched groups radiate from a central core was exploited as the MM side chain due to their increased steric hindrance and reduced MW compared to polymeric side chains (**Figure 10**a). As a result, this type of pendant chain can maintain the congestion required to extend the main chain backbone, while, at the same time, increase the accessibility of the MMs to the propagating polymer chain during synthesis. Such BBCPs have been reported to allow relatively easy access to higher DP polymers (up to a DP of 4000) while also offering faster kinetics for self-assembly, resulting in a high degree of order. Using dendronized BBCPs with a DP of 1500, the prepared films were reported to reflect near-infrared light up to 888 nm, which could be further extended upon annealing to 1223 nm, because of enthalpy-driven lamellae thickening. This class of BBCP was also applied to 3D printing, albeit with slightly different dendritic side chains, in order to produce complex structures with structural color (Figure 10c).[101] As such, adopting such dendronized wedge-like side chains presents a method

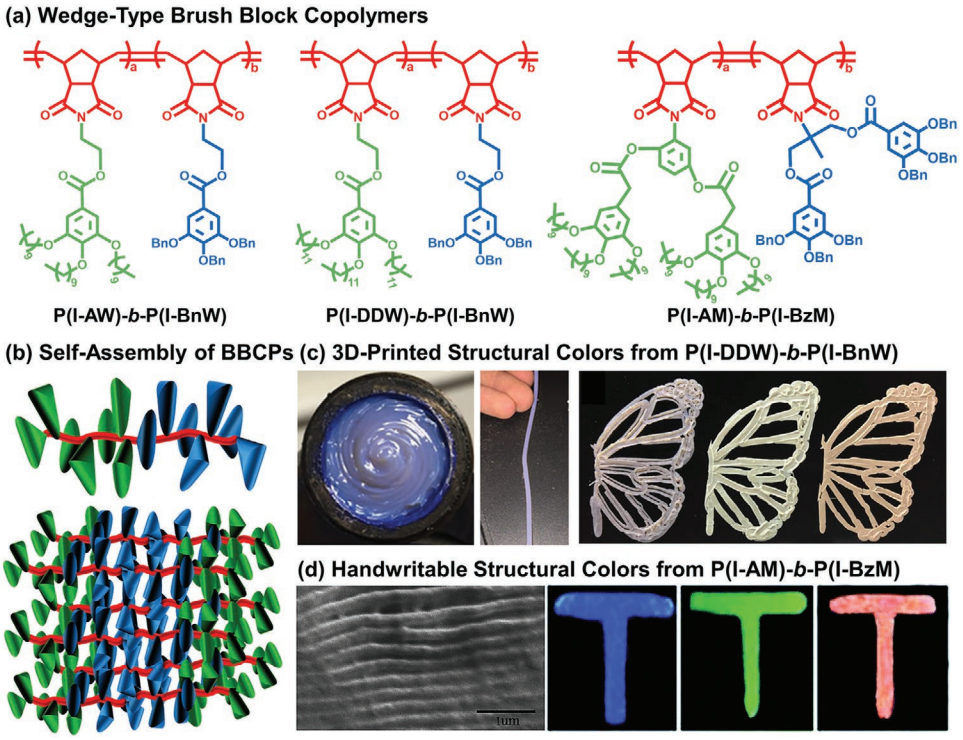

Figure 10. a) Three brush block copolymers based on wedge-type macromonomers. b) Schematic illustration of the self-assembly of wedge-based BBCPs. Reproduced with permission.[99] Copyright 2013, American Chemical Society. c) Structural colored designs obtained from 3D printing of P(I-DDW)-*b*-P(I-BnW). Adapted with permission.[101] Copyright 2017, American Chemical Society. d) Handwritten structural colors from P(I-AM)-*b*-P(I-BzM). Adapted with permission.[126] Copyright 2019, the Royal Society of Chemistry.

to decrease the steric hindrance during polymerization and therefore access huge DPs without sacrificing the rigidity of backbone.

Recently, two dendronized MMs (NB-AM and NB-BzM) were prepared with second-generation dendrons as side chains.[126] Through ROMP, these two MMs were sequentially polymerized together into poly(NB-AM)-*b*-poly(Nb-BzM) BBCP (Figure 10a). With these more complex side chains, the steric hindrance was promoted, stretching the norbornene backbone further and achieving more rapid self-assembly rates. As such, the self-assembly and formation of lamellar structures were achieved during the solvent evaporation process, without the need for further annealing (Figure 10b). When the total DP was increased from 400 to 1300, the domain spacings of the resulting lamellar structures changed from 110 to 523 nm, corresponding to vibrant colors from blue (403 nm) to red (668 nm) (Figure 10d), even reaching the infrared region (1231 nm). Due to the improved self-assembly kinetics and optical performance, dendronized BBCPs offer great potential in paint or as coating materials, and can further be extended to sensing applications by exploiting their responsiveness to swelling by solvents, such as alcohols.[127]

While it has been shown above that the side chain has a great influence on the domain spacing of photonic BBCP multilayers, it is only recently that the effect of the backbone on the BBCP self-assembly process and the resulting photonic structure has been explored.[128] Most norbornene-based moieties for ROMP can be broadly classified into two types of chemical structures, norbornene with modifiable pendant groups (N) and norbornenyl imide linked with activatable end-capping (I). Ren and co-workers compared these two structures, by synthesizing using ATRP MMs containing PS and poly(*tert*-butyl acrylate) (P*t*BA). The four combinations of the side-chain and backbone structure are referred to below as N-PS, N-P*t*BA, I-PS, and I-P*t*BA. Two BBCPs, poly(N-PS)-*b*-poly(N-P*t*BA) and poly(I-PS)-*b*-poly(I-P*t*BA), were prepared via ROMP. These, referred to respectively as poly(N) and poly(I), contain different backbones, but are otherwise prepared using the same parameters. Poly(I) demonstrated a higher glass transition temperature (T_g) than poly(N), indicating poly(I) is more rigid. The change in rigidity of the polymers also manifested in the thermal response of the formed lamellar structures. At high temperatures, the structures were no longer kinetically trapped and would therefore approach the equilibrium state. In this case, this is represented by an increase in domain spacing and reflection wavelength. For poly(I), the structural color was observed to shift from violet (360 nm) at room temperature to dark blue (450 nm) at 140 °C. In comparison, the maximum reflection wavelength achievable via thermal treatment for poly(N) was limited to 412 nm, which reflects the softer backbone of poly(N) compared to poly(I), leading to a less extended chain conformation at high temperatures.

The impact of backbone composition was investigated in more detail by Miyake et al.[129] As above, four MMs were prepared by combining the two backbone structures with two different polymer side chains, in this case, PS and PLA. However, in contrast to the study by Ren, BBCPs with mixed combinations of the backbones and the side chains were

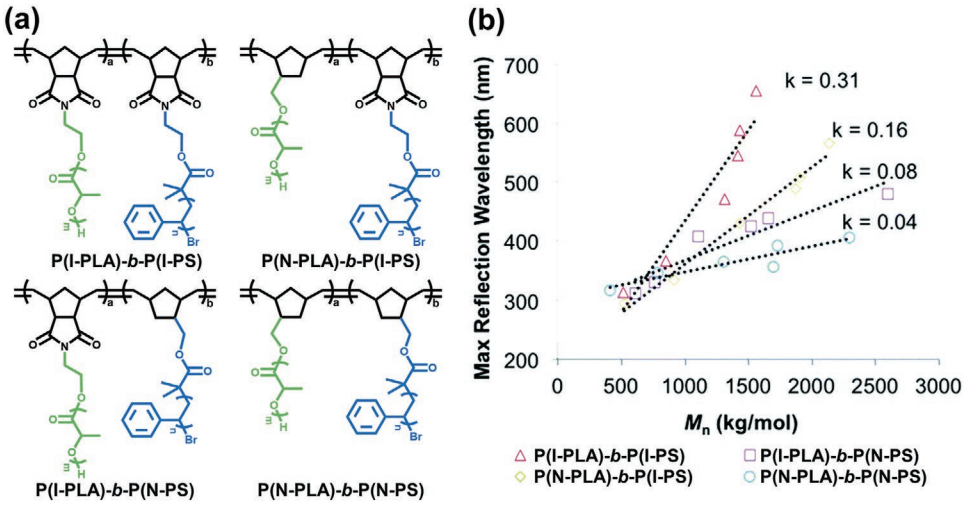

Figure 11. a) Four brush block copolymers with different backbones. b) A plot of the maximum wavelength of reflection of films from the four BBCP series against the M_n of each polymer (k = gradient of best fit line). Adapted with permission.[129] Copyright 2020, the Royal Society of Chemistry.

synthesized, resulting in four series of BBCPs with distinct backbone compositions but with equal molar ratio of the blocks. These are denoted as P(I-PLA)-*b*-P(I-PS), P(N-PLA)-*b*-P(I-PS), P(I-PLA)-*b*-P(N-PS), or P(N-PLA)-*b*-P(N-PS), as shown in **Figure 11**a. The lamellar structures were prepared using these BBCPs through thermal compression and annealing at 140 °C. Although, as expected, the maximum reflection wavelength increases with an increase of the MW or the DP for all types of BBCPs, the rate of increases varies for each type. For P(I-PLA)-*b*-P(I-PS), the reflection wavelength increased more effectively with the change of DP, and the others followed the order of P(N-PLA)-*b*-P(I-PS) > P(I-PLA)-*b*-P(N-PS) > P(N-PLA)-*b*-P(N-PS). As a consequence of the smaller rate of increase with DP, the maximum reflected peak wavelength for P(N-PLA)-*b*-P(N-PS) is 406 nm (violet), while that of P(I-PLA)-*b*-P(I-PS) can reach 655 nm (red-orange). However, using the I backbone also resulted in less well-aligned domains with greater variation in domain size, as measured by the full-width-half-max (FWHM) value of the reflection spectra. The FWHM of the P(I-PLA)-*b*-P(I-PS) spectra was 428 nm, while that for P(N-PLA)-*b*-P(N-PS) was only 153 nm. Through a detailed rheological study, it was concluded that the rigidity of the BBCP backbone is responsible for the ability to rapidly phase separate and assemble into lamellar structures with larger domain spacings and organize into well-aligned domains. When more rigid backbones were used, such as I, a more efficient interfacial arrangement process of the BBCPs occurred and as a result less energy input was required. In contrast, for P(N-PLA)-*b*-P(N-PS), especially for large MW, it did not readily produce well-ordered lamellar structures, with the efficiency of the self-assembly process decreasing as the DP increases.

Beyond directly tuning their chemical composition or the presence of additives, physical parameters, such as shear, have also been explored as a strategy to change the self-assembled microstructures of BBCP-based photonic multilayers. Rogers and co-workers prepared a highly concentrated polymer solution of P(N-PLA)-*b*-P(N-PS).[130] When shear was applied to the polymer solution, different colors were observed depending on the shear rate. At quiescence or low shear rate, the sample reflected a green color, corresponding to a lamellar structure with a domain spacing of 161 nm. Higher shear rates resulted in the distortion of the BBCPs and compression of the domain spacing, which, in turn, caused a blueshift. As such by controlling the applied shear other colors could be observed.

The effect of shear on the visual appearance is also important in the context of additive manufacturing, such as 3D printing. Diao et al. showed the possibility to print multiple colors with a single BBCP by simply changing the printing conditions.[131] The BBCP P(N-PDMS)-*b*-P(N-PLA) forms a weakly ordered micellar phase with multiple colors when drop-cast from solution (**Figure 12**a). However, when the solution was used in a 3D printer, a shear stress was applied to the polymer, altering the self-assembly behavior and resulting in the formation of lamellar structures that reflected structural color upon solvent evaporation (Figure 12b). By changing printing conditions, such as printing speed and substrate temperature, the lamellar structures were kinetically arrested at different stages in the assembly process, which led to controllable domain spacing across the full visible spectrum (Figure 12c). Combined with well-designed printing procedures, they showed that complex patterns with multiple colors could be printed (Figure 12d).

2.2.3. Understanding the Microphase Separation of BCPs

The self-assembly of either LBCPs or BBCPs is driven by microphase separation arising from an incompatibility between two chemically disparate polymer blocks.[132–135] It is widely understood that the morphology of the produced self-assembled structures, ranging from simple micelles to complex gyroids, depends on the shape, size, and ratio of the constituent blocks.[136–139] When the volume fractions of the two blocks are comparable, lamellar structures tend to be formed.[2,6] In contrast, more asymmetric BCPs tend to promote curved interfaces which, combined with the relative chemical incompatibility of

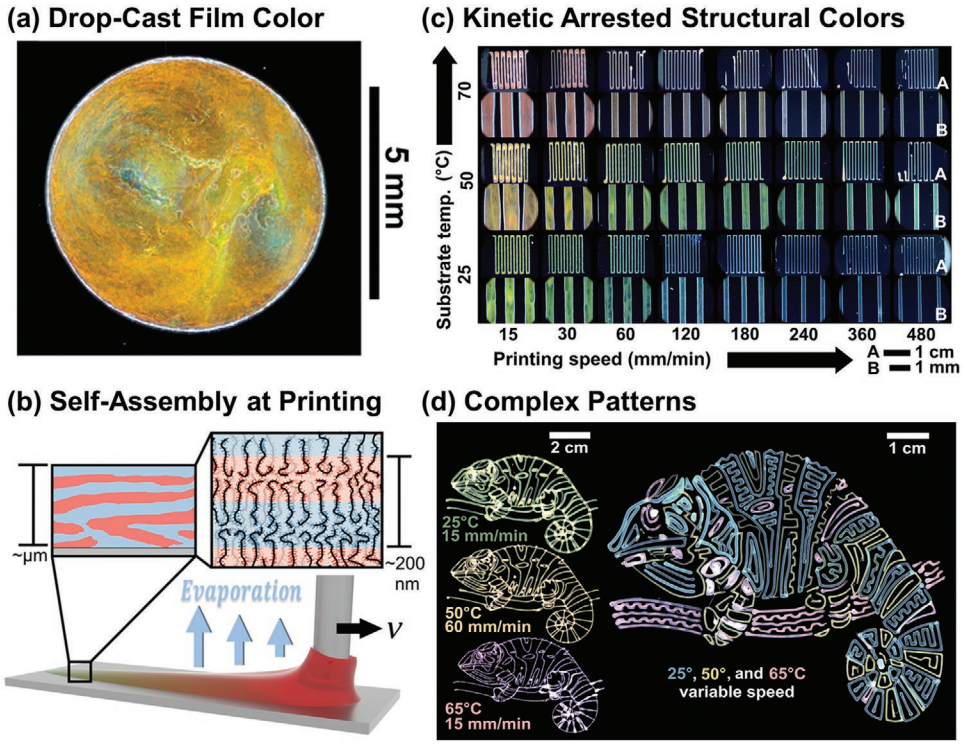

Figure 12. a) Microscope image of a drop-cast film from P(N-PDMS)-*b*-P(N-PLA). b) Schematic illustration of self-assembly during printing. c) Various structural colors are formed by controlling the printing speed and substrate temperature. d) Complex pattern printed. Adapted with permission.[131] Copyright 2020, The Authors, some rights reserved; exclusive licensee AAAS. Distributed under a Creative Commons Attribution NonCommercial License 4.0 (CC BY-NC).

the blocks with each other and the solvent, can lead to more complex architectures or higher-order structures.[140,141] Finally, it should be noted that the self-assembled structure can be concentration dependent: as the BCP concentration increases, it is possible to pass through several different phases, making the final architecture in the solid state not always easy to predict. So far, this review has primarily focused upon photonic structures formed from self-assembled lamellar architectures. However, the recent discovery of photonic glasses formed from the micelle-driven assembly,[142] as discussed in Section 3.2, shows that structures templated from other phases can also offer interesting optical properties.[10]

Focusing upon lamellae formed from LBCPs, the observed color in reflection can be tuned by the domain spacing. This spacing typically increases with the overall DP (which is proportional to MW) of the BCPs within a polymer series of the same monomer composition.[143–146] However, for the ultrahigh molecular weights required to access domain spacings large enough to produce a photonic response, the conformation of the LBCP in solution can make predictions of the domain spacing challenging. Furthermore, the relationship between the DP and the domain spacing may not be linear and is typically unknown. Finally, when coloration is achieved by swelling, the choice of solvent or amount of dopant can dominate over the underlying architecture. In contrast, while BBCPs have an additional complexity in terms of the composition and DP of the side chains, the increased rigidity of the backbone this structure affords typically results in linear relationships between DP and the peak reflected wavelength.[110,124,147,148] However, the exact relationship again varies between copolymer systems, as differences in terms of side chain conformation, crystallinity, and volume all have an effect on the domain spacing. Finally, it is also important to take the nature of the packing of the BBCPs within each domain into account, whereby any overlap beyond the idealized end-to-end packing model will lead to a smaller domain size than that predicted from simple BBCP length measurements, by, e.g., light scattering. As such, how all these factors combine to determine the domain size is not yet well understood and is deserving of further investigation to enable more rational polymer design.

3. The Self-Assembly of Block Copolymers in Confinement

In the previous sections, the role of chemical composition and processing conditions upon the optical properties of a photonic BCP multilayer were discussed in the context of films and coatings. However, recently it has been shown that the geometry can also contribute to the overall optical response, with soft confinement within micron-scale droplets allowing for hierarchical architectures to be produced. Constraining the self-assembly process within a confined environment offers several advantages: i) It can exploit the effects of unstable interfaces, lost entropy, and symmetry breaking to allow the fabrication of novel architectures that are often challenging to obtain when processing BCPs into films from a polymer melt or solution.[149] Also, kinetic effects can be exploited to trap nonequilibrium

structures. ii) Confinement provides an additional degree of hierarchy (in shape, morphology, or surface property) that can enrich the optical response.[150] However, despite many examples of polymeric nanomaterials fabricated via the confined self-assembly of BCPs,[151–154] there are only a few examples that exploited polymeric systems large enough to assemble into structures that could generate a photonic effect.

Historically, confined self-assembly has been exploited to produce photonic structures using colloidal systems,[155–159] typically constrained within micron-scale droplets as an emulsion or dispersion in air.[23,160,161] The resultant particles (often called photonic pigments) consist of hierarchical spherical objects with dimensions of the order of several tens of microns, with an internal architecture which is periodically structured on the scale of the wavelength of visible light. However, recently it has been reported that by simply dissolving suitable BCPs into appropriate solvents, compartmentalizing into spherical droplets via emulsification and then allowing for evaporation-induced self-assembly to occur, analogous photonic particles can be produced. In the following sections, we discuss the two main types of photonic pigments obtained by BCPs in confinement: concentric multilayers (formed from radially aligned lamellae) and photonic glasses (templated by micelles).

3.1. Concentric Multilayers

Linear BCPs typically form a planar-aligned lamellar structure resulting in a structurally colored film, however within spherical confinement the same self-assembly process can be directed to form a radially-aligned lamellar structure, resulting in a concentric photonic multilayer particle (i.e., a photonic pigment). An example of such a hierarchical photonic structure was obtained by Zhu et al.,[162] who emulsified PS-*b*-P2VP within chloroform-in-water droplets, which subsequently underwent evaporation-induced self-assembly to form concentric lamellar particles (**Figure 13**). However, PS-*b*-P2VP with an MW of 265 kDa does not produce any structural color in the visible range (Figure 13b), so swelling was employed to increase the domain size. Water and ethanol are both good solvents for P2VP and by swelling in a mixture of these solvents and controlling the ratio, visible color from blue (450 nm) to red (670 nm) was achieved (Figure 13c). Furthermore, by changing the degree of swelling of the P2VP block by altering its protonation via pH, the reflected wavelength could also be redshifted by over 320 nm, leading to a reflection through the entire visible spectrum. However, the authors observed that the swelling only happened in the first several layers from the surface rather than the whole microsphere, regardless of the pH or the amounts of solvent added. Two reasons were proposed for this observation: the PS layers block further solvent permeation, while the high stress induced by the increasing curvature towards the center of the droplet lowers the accessibility of solvents inwards.

The high curvature of the concentric lamellae near the core of spherical droplets also disfavors BCP self-assembly, with the resultant inhomogeneous domains leading to poly-chromaticity and broader reflection peaks. To bypass these issues, photonic capsules with a hollow core were proposed.[163] Exploiting droplet-based microfluidics and spontaneous emulsification,

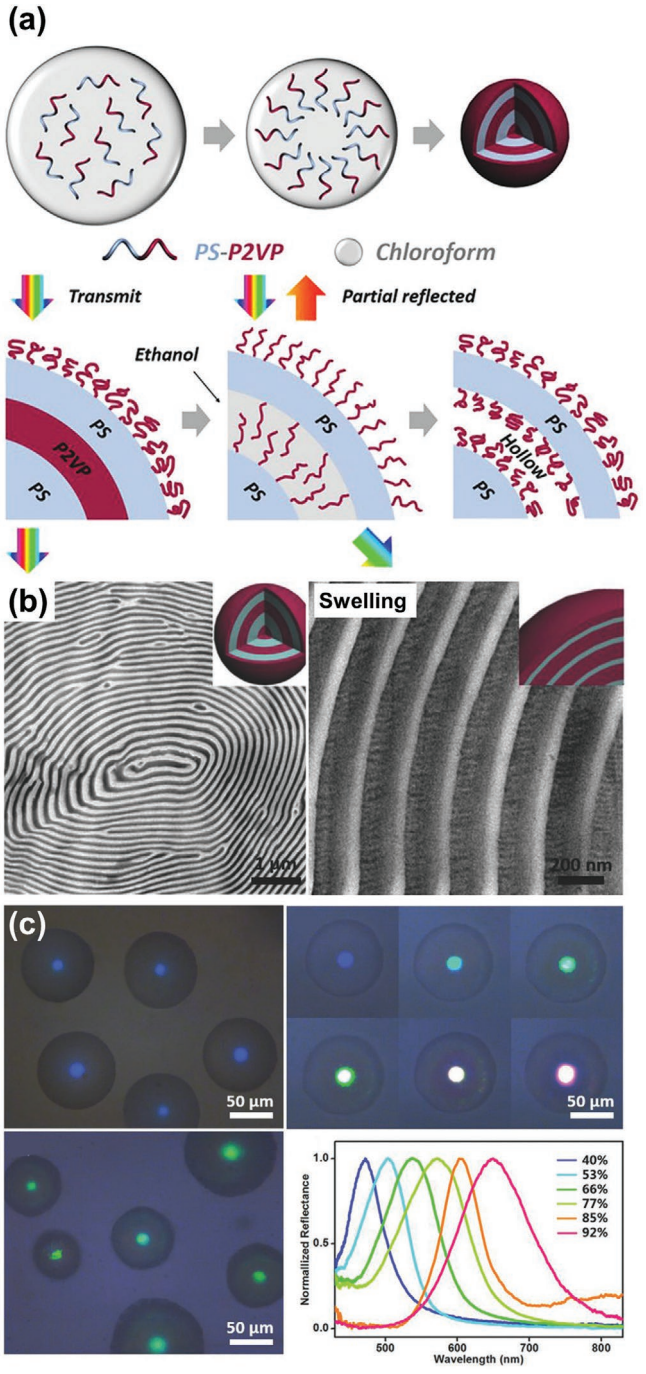

Figure 13. Preparation of photonic pigments based on PS-*b*-P2VP and the control of reflected color: a) schematic illustration of the preparation of photonic pigments and their swelling process with solvents; b) SEM images of the internal structures of these photonic pigments; c) the optical microscopy images of the photonic pigments under different conditions and their normalized reflectance spectra. Adapted with permission.[162] Copyright 2018, Wiley-VCH.

a water-in-oil-in-water (W/O/W) double emulsion was produced, with the PS-*b*-P2VP confined to the outer droplet (**Figure 14**a). By tailoring the parameters of the emulsification process, microcapsules with lamellar concentric shells were

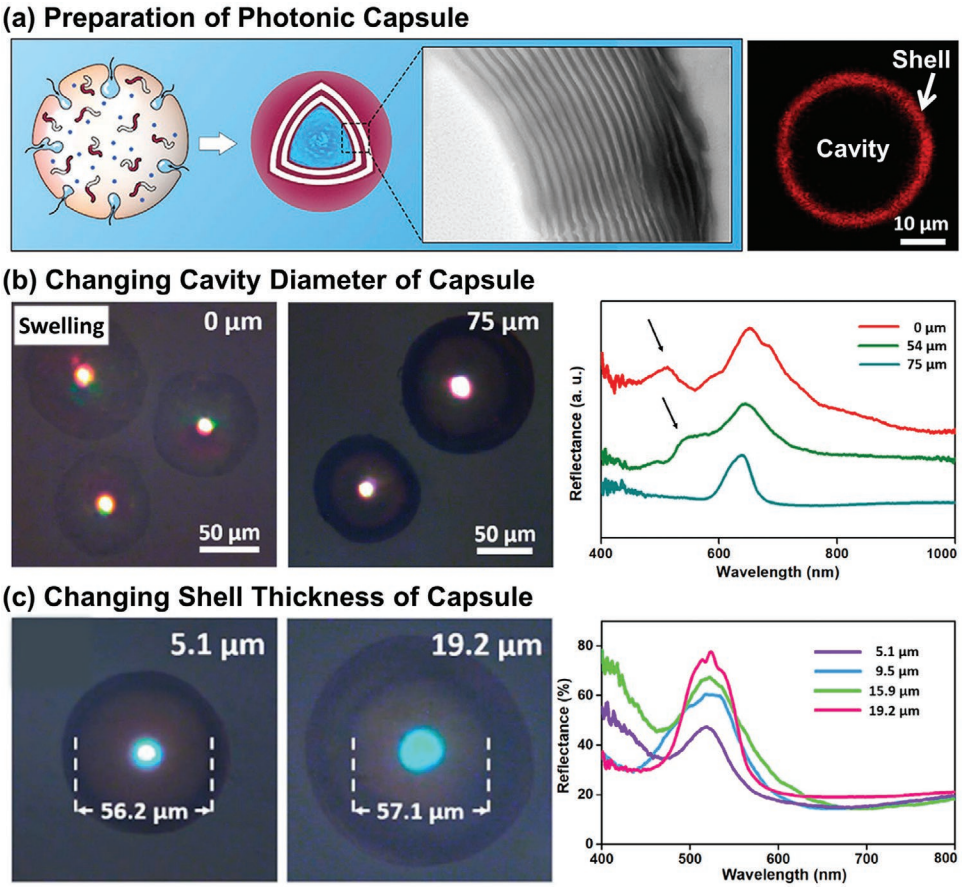

Figure 14. a) Preparation of hollow photonic microcapsules. b,c) Microscope images and corresponding reflection spectra of the photonic capsules with different cavity diameters and different shell thicknesses. Adapted with permission.[163] Copyright 2020, American Chemical Society.

obtained after complete evaporation of the outer droplet. At a pH of 6.8, the resultant photonic capsules reflected a bright blue color (422 nm). Decreasing the pH value can protonate the P2VP block, rapidly enlarging the domain spacing of P2VP and causing a redshift to 650 nm. A richer palette was then achieved by altering the MW of the constituent PS-*b*-P2VP and by blending these polymers in different ratios. By controlling the cavity diameter and shell thickness, the optical appearance of these photonic microcapsules, in terms of reflectance and monochromaticity, was improved when compared to the analogous solid microparticles (Figure 14b,c).

A more robust strategy has been reported by the Zhu group to tune the structural colors of PS-*b*-P2VP photonic pigments, leading to more uniform concentric photonic multilayers.[164] Using an emulsion method, a PS-*b*-P2VP with MW of 438 kDa was used to obtain concentric multilayers reflecting blue prior to any post treatment. Each block was then swelled selectively: P2VP by 3-*n*-pentadecylphenol (PDP), which forms supramolecular interactions with P2VP via hydrogen bonding, and PS by polystyrene homopolymers (hPS). By swelling both blocks, the size ratio between the two domains in the lamellae was retained, which is critical to the formation of a good photonic multilayer. Moreover, the domain spacings of the photonic pigments were greatly enlarged, resulting in an effective change in the reflected wavelength from 422 nm to 806 nm.

Despite these advancements, it is still challenging using LBCPs to sharpen the broad reflection peaks that result from misaligned and irregular lamellae, especially for the large domain spacings required to produce red pigments. This intrinsic limitation of LBCPs is due to the high degree of entanglement that occurs during self-assembly, which, as discussed above, can be avoided by using BBCPs. Concentric multilayers based on BBCPs were reported for the first time in 2019 by Song et al.[111] In this study, P(N-PS)-*b*-P(N-PDMS) BBCP was fabricated into photonic spheres for pigments via confined self-assembly within emulsified chloroform droplets (**Figure 15**a). The rapid microphase separation of different polymer segments upon the complete removal of solvent resulted in a concentric lamellar interior structure giving rise to vivid structural colors. By changing the MW or blending BBCP with different MWs, the reflected color of the particles could be tuned across the visible spectrum, from blue to red (Figure 15b–d). These concentric multilayers can be further altered by applying external stimuli, with the color observed to change when exposed to different solvents. In this work, the reflected light displayed high intensity, up to 100% of the incident light and this is a result of the long-range order of the highly uniform lamellar structure (Figure 15d–f). While the reflected color was found to be size independent, the intensity initially increases with the particle diameter, corresponding to a larger number of layers in

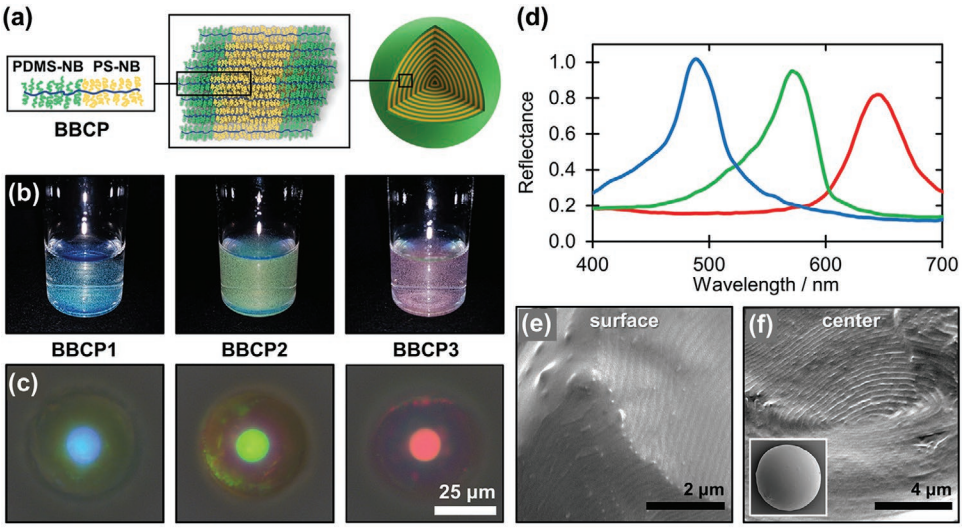

Figure 15. a) Photonic pigments based on lamellar brush block copolymers. b) Photographs of photonic pigments suspensions in water formed by different brush block copolymers. c) Reflection optical microscopy images of the microparticles and d) corresponding reflectance spectra. e,f) SEM cross-section images of a single photonic pigment, showing the well-ordered, concentric lamellae. Adapted with permission.[111] Copyright 2019, American Chemical Society.

the concentric multilayer. However, the reflectance saturates for particles larger than 5 μm, and as such became size independent. Using BBCPs instead of LBCPs also seems to further impact the color purity: for a red reflection, the full-width-half-max (FWHM) value of a LBCP is usually more than 100 nm, while for BBCP it can be reduced to about 50 nm. While the FWHM depends also on the refractive index contrast between the blocks and the backbone construction, these results suggest that overall, the higher degree of ordering that can be achieved with BBCPs could result in photonic pigments with greater color purity.

The boundary condition of the confined environment plays an important role in templating the formation of lamellar structures, which affects the degree of ordering, and therefore the final optical properties. In BCP films, the substrate can be functionalized for better ordering of the lamellar structures.[38,43,53,71,72] An analogous method in confined systems is to manipulate the interface through the surfactant employed. Zhu et al. presented an approach using poly(vinyl alcohol) (PVA) to stabilize an emulsion of PS-*b*-P2VP.[165] The affinity of the P2VP block to the hydrophilic droplet interface ensured that P2VP is the outermost layer and that the growth of lamellar structures occurs inwards from the surface. Song et al. further investigated the effect of surfactant on the formation of BBCP lamellar structures within droplets by comparing a range of surfactants.[111] When PVA was employed it was observed that the lamellar structure formed first at the liquid–liquid interface and gradually extended to the center. This indicates that the initial stabilization of the interface by BBCP templates the subsequent lamellar self-assembly, giving rise to a hierarchical lamellar particle. However, when ionic surfactants such as sodium dodecyl sulfate (SDS) and cetrimonium bromide (CTAB) were used, they preferentially stabilize the droplet interface instead of the BBCP. As such the BBCP was not initially organized at the droplet interface and consequently lamellar formation occurred as a bulk process within the droplet volume. As a result, a disordered polydomain lamellar structure was formed, resulting in diminished optical properties.

The importance of the interface upon the final structure was affirmed by Kim et al.[166] BBCPs with different DPs were synthesized via ROMP using norbornenyl MMs with dendronized side chains, I-AW and I-BnW. Emulsions were used to template the confined self-assembly of these BBCPs. To optimize the interaction between BBCPs and surfactants, two dendronized surfactants containing the side chains of AW and BnW were prepared, named as S_{AW} and S_{BnW}. When a single dendronized surfactant was used, S_{AW} or S_{BnW} would provide strong preferential interaction between the corresponding AW or BnW block and the droplet interface, resulting in the inward growth of a radially aligned lamellae. However, a mixture of the two surfactants allowed for the concurrent affinity of the two blocks to the droplet interface, which led to axial stacking of the lamellae (**Figure 16**a,b), giving rise to ellipsoidal particles with a striped multilayer photonic structure. The formation of an ellipsoidal geometry is attributed to elongation to release the entropic penalty of bending the BBCP chains, as achieved by increasing the surface area and reducing the curvature of the axially stacked lamellar layers. The structural color of the striped multilayer varied between 369 to 659 nm by changing the DP of the BBCP (Figure 16c). While concentric multilayer microspheres are uniformly colored in solution, these ellipsoidal, axially aligned multilayer particles behave effectively as small flakes of a planar multilayer film. As such the reflection is always specular, resulting in a variety of distinct colors (i.e., iridescence) that arise from the specific orientation of each individual particle (Figure 16d–f). However, due to the decrease in intensity at higher angles arising from the ellipsoidal geometry, the overall visual appearance of the particle dispersion is dominated by the color reflected at normal incidence. Furthermore, by incorporating Fe_3O_4 magnetic nanoparticles, the authors demonstrated that the particles could be aligned in a magnetic field. As shown in Figure 16g, when the detection angle and the illumination angle

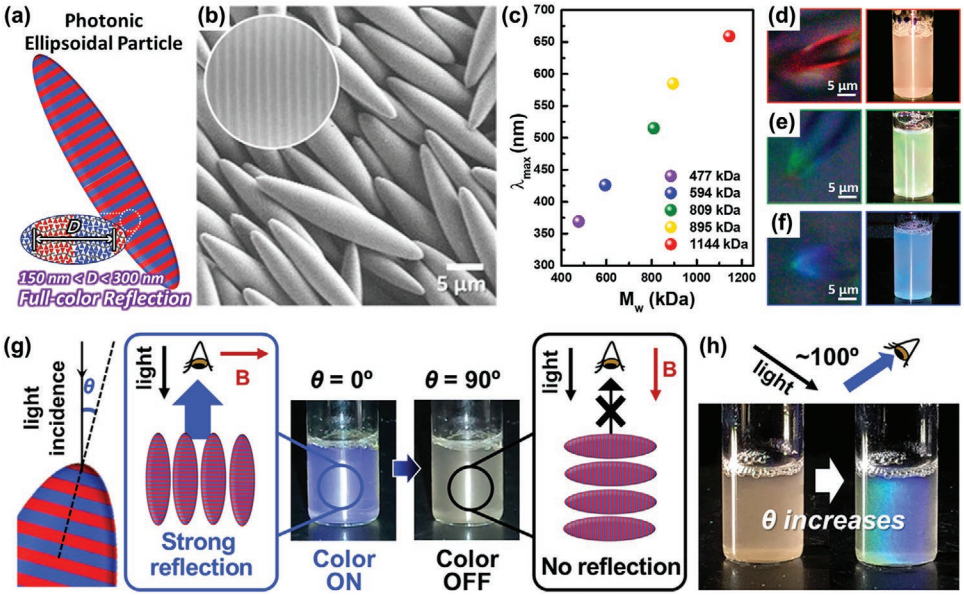

Figure 16. Striped multilayer particles formed by the self-assembly of P(I-AW)-*b*-P(I-BnW) and their optical response. a) Schematic illustration and b) SEM images of the ellipsoidal particles. c) Plot of λ_{max} as a function of MW of BBCPs. d–f) Reflection images of the ellipsoidal particles and photographs of the corresponding particle suspensions in water. g,h) On/off or blue-shift coloration of the particle suspension by precisely controlling the particle orientation. Adapted with permission.[166] Copyright 2020, American Chemical Society.

are the same, the particles can display a violet color or appear colorless when the stacking direction of the multilayer is respectively aligned parallel or perpendicular to the viewing direction. As such, an on/off optical response was achieved, allowing for the optical appearance to be externally switched. Finally, the length of the backbone has been recently shown to influence the formation of the final ordering within the particle.[167] It was reported that increasing the backbone length will increase the entropic penalty of stretching or bending the BBCPs into curved lamellae, which will eventually overwhelm the enthalpic contribution from stabilizing the droplet interface. This results in axial stacking of the lamellae into an ellipsoidal particle becoming preferred for high MW BBCPs or for very small droplets, where the effects of the confinement geometry are amplified.

3.2. Inverse Photonic Glasses

Isotropic correlated photonic structures, often referred to as photonic glasses, are interesting due to the potential for noniridescent structural color, however they are generally challenging to fabricate. In such systems, the coloration is the result of both coherent scattering and Mie scattering induced by the short-range order associated with the arrangement of nanoscale particles (or pores in the case of inverse photonic glasses).[168] Recently, such a correlated photonic structure was obtained using BBCPs in the confined environment of a microdroplet to produce photonic pigments.[142] A low MW BBCP with a DP of 72, poly(I-PS)-*b*-poly(N-PEO), was used to prepare an inverse photonic glass. In this case, the small molecular weight of the BBCP cannot produce structural coloration in the visible range when forming a lamellar structure. In contrast, when a solution of this BBCP in toluene was homogenized into an emulsion within an aqueous PVA solution, micellization of the BBCP within the resultant toluene droplets followed by subsequent swelling with water leads to the formation of internal nanoscale droplets. Upon drying they tightly pack within the larger toluene drop to form a correlated disordered network of BBCP-stabilized nanodroplets, with pores formed upon complete loss of solvent (**Figure 17**a,b). The coloration of the resulting porous particles can be changed by varying the initial amount of water within the toluene droplet, which dictates the final pore size (Figure 17c,d), with the wall thickness correlated to the length of the BBCP itself. This was achieved by tuning the emulsification conditions, such as homogenization speed and duration. Therefore, with this technique, the authors were able to prepare vibrant colors across the full visible range, using only one BBCP with a defined and relatively low MW.

It has since been shown that for fixed emulsification conditions the average pore diameter and therefore the reflected color of porous BBCP pigments can also be tuned by changing the polymer backbone length.[169] When the DP of the BBCPs was increased from 89 to 115, the reflected colors can be tuned from violet to red, shifting further to infrared with a DP of 132. The low polydispersity and high degree of short-range order in these internal pores, which are beneficial for the formation of structural color, were attributed by the authors to the rigidity of the BBCP. Finally, oxidation can also be used to tune the structural color of porous BBCP particles.[170] In this case, a BBCP with an oxidation-responsive ferrocene group incorporated within an I-PEO layer was used to prepare inverse photonic glass pigments. When oxidized by hydrogen peroxide (H_2O_2), the ferrocene cation enhanced the hydration of the hydrophilic I-PEO, causing the block to grow in size and occupy more space at the interface of the internal water droplet. This, in turn, caused the micelles to expand in order to reduce the steric

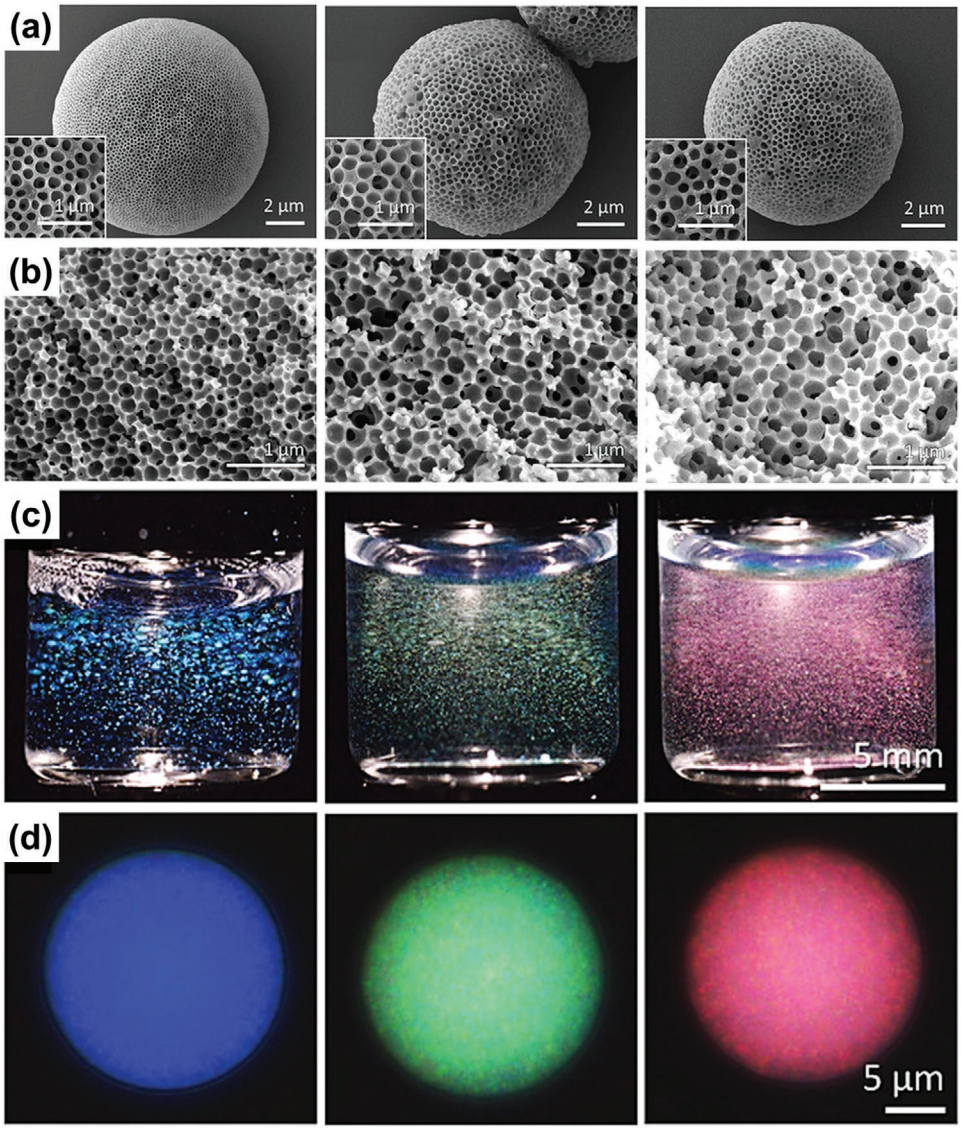

Figure 17. a,b) Scanning electron microscope images of the surface and internal structure of the BBCP inverse photonic glass particles, emulsified under different conditions. c) Corresponding photographs of porous photonic pigment dispersions under direct illumination, and d) microscope images of individual microspheres. Adapted under the terms of the CC-BY license.[142] Copyright 2020, The Authors, published by Wiley-VCH.

repulsion between the PEO blocks, leading to an increased pore size and redshift of the reflected structural color. Through controlling the degree of oxidation by molar ratio and reaction time between ferrocene and H_2O_2, a full spectrum of colors was obtained. This strategy could be replicated in BBCPs with a range of DPs from 56 to 108. In addition, this photonic structure was recently employed in ultra-trace quantitative detection, by incorporating aggregation-induced emission luminogens (AIEgens) in the side chains of the BBCPs.[171]

3.3. Understanding the Optical Response of BCP-Based Photonic Pigments

In this review, the formation of a variety of photonic structures from block copolymers has been shown, namely planar multilayer, concentric multilayer, and inverse photonic glass. While methods to tune the reflected wavelength have been discussed, the overall optical appearance, especially the angular dependence of the wavelength (iridescence) has not been addressed. While the angular dependence of the color reflected by a planar multilayer can be easily understood in terms of Bragg's law,[172,173] the case for concentric multilayer and photonic glass structures is more complex and multiple factors need to be considered.

The Ewald's sphere is a geometric construction frequently used to predict the angular response of materials in X-ray diffraction. However, it can also be useful to predict the optical response of various photonic structures while accounting for observation angles and illumination conditions.[174,175] As the Ewald's spheres are constructed in reciprocal space, the reciprocal structures of a planar multilayer, a concentric multilayer,

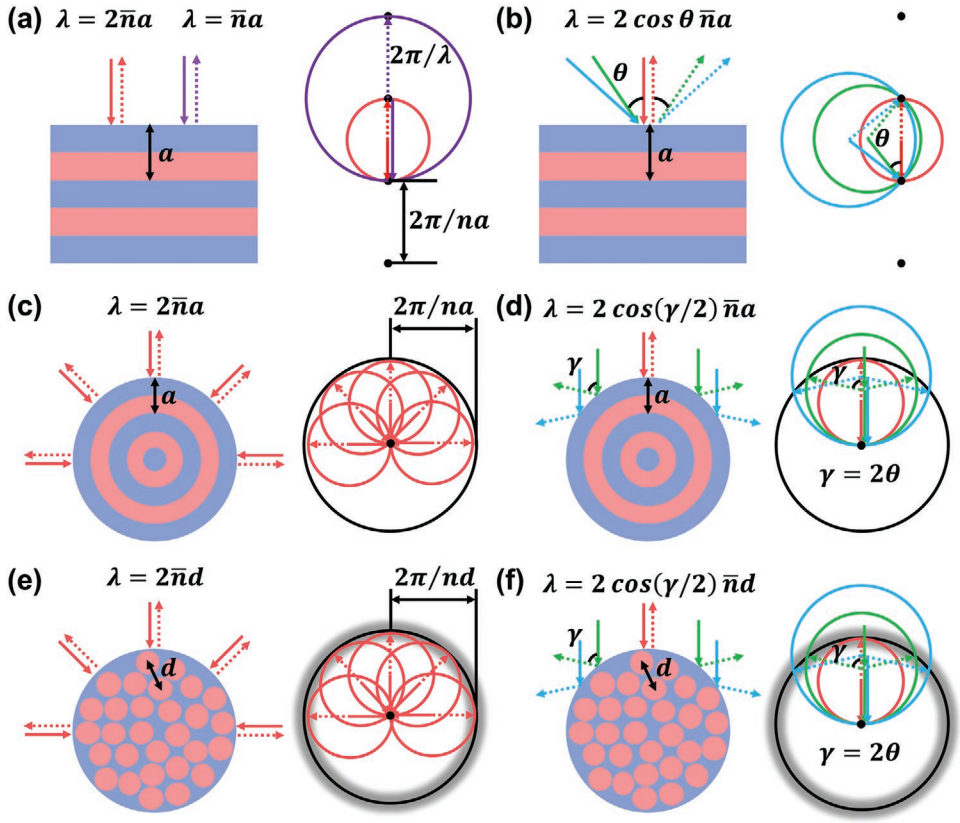

Figure 18. Comparison of the angular dependence of the optical response under different illumination conditions for a,b) planar multilayer, c,d) concentric multilayer, and e,f) photonic glass. Each pair of schematics describe the light path in real space (left) and also in reciprocal space (right). The directions of incident and reflected light are indicated by solid and dashed arrows, respectively. The black nodes and circles represent the reciprocal structures. The colored circles ($r = 2\pi/\lambda_0$, λ_0 is the wavelength in vacuum) are the 2D projection of Ewald's spheres. The Bragg condition is satisfied when the Ewald's sphere intersects with the reciprocal structure, resulting in reflection from the structure. Design based on ref. [174], published under the terms of the CC-BY license. Copyright 2018, OSA Publishing.

and a photonic glass are considered in **Figure 18**. The reciprocal lattice of a planar multilayer consists of a series of nodes that are aligned to the stacking direction of the multilayer, with the nodes spaced by $2\pi/n_{\text{eff}}a$, where a is the lattice constant of the multilayer and n_{eff} is the effective refractive index of the multilayer (Figure 18a).[176] The reciprocal structure of the concentric multilayer is then a series of spheres that are projected as circles in 2D (here only the innermost ring is drawn for simplicity, Figure 18c). The radii of the rings are $2m\pi/n_{\text{eff}}a$, where m is any positive integer. Finally, the reciprocal structure of the photonic glass is similar to the concentric multilayer, but often only a single sphere exists due to the weak ordering. The radius of the ring is $2\pi/n_{\text{eff}}d$, where d is the correlation length and n_{eff} is the effective refractive index of the glass. The boundary of the ring is blurred as the positional correlation is a distribution instead of a discrete value (Figure 18e).[177] It should be noted that the geometrical confinement of the photonic glass has no impact on the reciprocal structure, whether it is a film or a sphere.

The Ewald's sphere (projected as a circle in 2D) for light with vacuum wavelength λ_0 is constructed by drawing a circle that starts with the origin of the reciprocal space and has the radius of $2\pi/\lambda_0$. When the Ewald's sphere intersects with the reciprocal structure, the Bragg's condition is satisfied. In this case, the wave vector of incident light is drawn from the center of the Ewald's sphere to the origin of the reciprocal space (solid arrow), while the wave vector of reflected light is drawn from the center of the Ewald's sphere to the intersected point between the reciprocal structure and the Ewald's sphere (dashed arrow).

Figure 18a illustrates the longest wavelength ($\lambda = 2n_{\text{eff}}a$) that can be reflected by a planar multilayer where the Ewald's sphere with the smallest radius ($r = \pi/n_{\text{eff}}\,a$) intersects with the reciprocal lattice points. Additionally, the second-order reflection ($\lambda = n_{\text{eff}}a$) is represented when the Ewald's sphere with double the radius ($r = 2\pi/n_{\text{eff}}\,a$) intersects with the reciprocal lattice points. When the first-order reflection is at 650 nm (red), the second-order reflection would be at 325 nm (UV), so the second-order reflection is usually outside the visible spectrum and does not impact the visual appearance (although it has been observed upon significant swelling of a BBCP photonic pigment).[111] Ewald's spheres with intermediate radii ($\pi/n_{\text{eff}}a < r < 2\pi/n_{\text{eff}}a$) need to shift outside the nodal plane to keep intersecting with the lattice points (Figure 18b). Therefore, a larger incident angle θ is required to reflect light with a shorter wavelength, resulting in the observed iridescent optical response under direct illumination.

Figure 18c,e illustrates the angular independent optical response when the concentric multilayer and photonic glass

structures are illuminated uniformly from all directions (i.e., under diffuse illumination). The longest wavelength ($\lambda = 2n_{\text{eff}}a$ for concentric multilayer or $\lambda = 2n_{\text{eff}}d$ for photonic glass) is reflected back in all directions, giving a consistent, noniridescent, visual appearance across all viewing angles. However, when the concentric multilayer and photonic glass are directly illuminated from a single direction, as in Figure 18d,f, the light is dispersed and reflected to a wide range of angles, with the shorter wavelength reflecting at a higher angle, resulting in iridescence. As such, by constraining the anisotropic multilayer into a concentric sphere, its optical properties are changed such that it behaves isotopically with respect to the observer. In contrast, the photonic glass structure is inherently isotropic, such that its optical properties are independent of any geometrical confinement.

The relationship between the reflected wavelength and angle of reflection of the three geometries are:

$$\text{Planar multilayer: } m\lambda = 2n_{\text{eff}}a\cos\theta \quad (1)$$

$$\text{Concentric multilayer: } m\lambda = 2n_{\text{eff}}a\cos(\gamma/2) \quad (2)$$

$$\text{Photonic glass: } m\lambda = 2n_{\text{eff}}d\cos(\gamma/2) \quad (3)$$

There are a few notable differences between these three geometries. First, comparing the planar multilayer to the concentric multilayer and photonic glass; sample orientation has no impact on the reciprocal structure of the latter two, so the optical response will be unchanged upon rotating the sample. However, rotating a planar multilayer also rotates the reciprocal lattice and consequently changes the optical response. Second, the reflection from the planar multilayer is always specular, while the reflection from the concentric multilayer and photonic glass is off-specular. Third, the planar multilayer always reflects backward, while the other two structures can reflect/scatter in the forward direction for short wavelengths. Furthermore, they disperse the same range of wavelengths ($\lambda \subset [2n_{\text{eff}}a\cos 90°, 2n_{\text{eff}}a\cos 0°]$) into a larger range of angles ($\gamma \subset [0°, 180°]$) than planar multilayer ($\theta \subset [0°, 90°]$), which explains why the photonic glass displays a weaker iridescence effect than for the case of a planar multilayer.[178] Last, comparing the photonic glass to the concentric multilayer, the former inherently has broadened reflectance peaks when multiple Ewald's spheres with different radii all intersect with the blurred circle to yield the incident and reflected wave vectors of the same direction but different wavelengths. The Ewald's sphere method also explains why a multilayer film containing multiple tilted domains is less iridescent, as their reciprocal structure more closely resembles that of the concentric multilayer.[109,179] It is also worth noting that the structural color of a photonic glass arises from both resonant Mie scattering of the scatterers (form factor) and coherent interparticle interference (structure factor). While the wavelength-dependence of the reflectance signal resulting from Mie scattering is not angular dependent,[180] it typically shows an ultraviolet-blue wavelength contribution.[168] As such, the above discussion only considers the optical appearance arising from the coherent interparticle interference component, which follows Bragg's law.

The Ewald's sphere description has shown that photonic materials with similar reciprocal structures produce a similar macroscopic optical response. However, Figures 15 and 17 demonstrate drastically different reflection images for concentric multilayer and photonic glass structures when observed under a bright-field optical microscope, where the numerical aperture of the objective lens determines both the illumination angle and collection angle. For the concentric multilayer, color is only observed as a spot at the center of each particle. This can be explained by considering the concentric multilayer as locally a series of planar multilayers that tilt along the curvature of the microparticle (**Figure 19**a1-4). As a multilayer always reflects in specular direction, light incident upon highly tilted multilayers is reflected outside the numerical aperture of the objective lens and as such not detected. In contrast, the inverse photonic glass displays uniform color across the entire cross-section in bright field. Here, the curvature of the microsphere has no impact on the internal photonic glass structure, so the reciprocal structure is consistent anywhere it is illuminated, which gives rise to a consistent optical response across the entire cross-section (Figure 19c2). Figure 19b1-4 illustrates how to incorporate a range of illumination and collection angles in the Ewald's sphere construction. Here, the illumination cone is shaded in yellow and starts on the origin of reciprocal space, while the detection cone is shaded in purple and starts on the reciprocal lattice point that intersects with the Ewald's sphere. Light can only be detected when the wave vector of the incident light originates within the illumination cone, and the wave vector of the reflected light points towards the collection cone. At the center of the concentric multilayer, a range of wavelengths are detectable (Figure 19b2). However, upon moving away from the center, light at shorter wavelengths is reflected outside the detection cone due to the high tilt of the multilayer (Figure 19b3,b4). As such, there is a boundary where only the longest wavelength ($\lambda = 2n_{\text{eff}}a$) is detectable, and beyond this boundary no reflected light enters the collection cone. In contrast, for the photonic glass, multiple collection cones exist along the circle in the reciprocal space with the longest wavelengths across the full cross-section of the particle (Figure 19c3). Upon decreasing the wavelength, the reflected light rapidly points outside the collection cone due to the large reflection angle ($\gamma = 2\theta$), causing the total detectable light to contain only a small range of wavelengths (Figure 19c4), allowing for strong color purity.

4. Conclusions and Prospects

This review provides an overview of the diversity of photonic materials that can be self-assembled from block copolymers, with particular focus upon the recent progress in producing functional photonic films and the development of hierarchical photonic pigments. The latter is particularly interesting as they offer a complex optical response that cannot be achieved with planar architectures. Finally, the interesting optical properties of BCP photonic pigments, such as noniridescence, were discussed and explained using an Ewald's sphere construction.

By exploiting rapid self-assembly kinetics and straightforward routes to tune the reflected color, BCP-based photonic materials offer many advantages over competing bottom-up

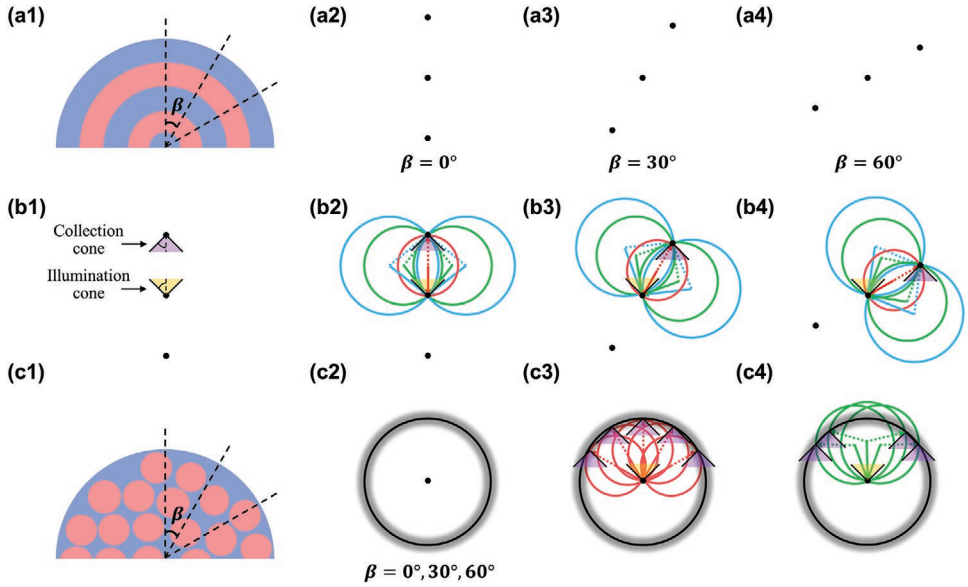

Figure 19. Using an Ewald's sphere construction to predict the microscopic optical appearance of photonic microspheres. a1–a4) A microsphere with containing a concentric multilayer structure can be approximated locally to a series of planar multilayers with different tilts. b1) The illumination cone and collection cone of the microscope objective lens remain the same in the reciprocal space. Wave vectors of the incident light and reflected light need to be within the illumination and collection cones for the light to be detected under the microscope. b2–b4) The higher tilt of the multilayer, as described in a2–a4) results in a smaller overlapping angle of the illumination and collection cones, which narrows the band of detectable wavelengths. c1,c2) The local reciprocal structure of a microsphere with a photonic glass structure remains the same across the entire volume. c3) Light with the longest wavelength ($\lambda = 2n_{\text{eff}}a$) is detectable throughout the entire overlapping angles of illumination and collection cones. (c4) When the wavelength decreases, the wave vector of the reflected light rapidly points outside the collection cone due to a large reflection angle ($\gamma = 2\theta$).

approaches (e.g., colloidal photonic crystals).[159] However, some fundamental questions have not been fully addressed. In particular, how intrinsic parameters of the BCPs (e.g., chemical composition, backbone DP, and side chain DP for BBCPs) and extrinsic parameters (e.g., solvent or dopants) affect i) the thermodynamics and kinetics of phase separation, and ii) the subsequent formation of the self-assembled photonic structure and its corresponding optical performance. By analyzing the contribution of each parameter across a wide range of copolymer systems and solvents, it should be possible to elucidate and generalize the relative importance of each property in determining the resultant photonic structure and its optical performance. Such a meta-analysis would allow the community to move from identifying trends within a single copolymer–solvent system, to the rational design of new functionality or higher-performing photonic materials by exploiting predictable polymer behaviors.

Block copolymer-based photonic systems have already been demonstrated to be compatible with additive manufacturing methodologies, such as ink-jet and 3D printing,[76,101,113,126] or for direct application as photonic pigments.[111,142,162] In general, the applications envisioned for BCP-based photonic materials center around two strategies: i) large-area coloration and ii) smart stimuli-responsive devices. As a colorant, BCPs could not only be employed as a continuous film but also in the form of a pigment within a formulation (e.g., in paints and cosmetics), with the latter envisaged in either platelet or spherical geometries. However, in all use cases the lack of scalable and cost-effective production methods for these polymers remains the limiting factor for large-area coloration, with most publications currently only reporting synthesis on the scale of a few hundred milligrams and exploiting expensive catalysts. As such new synthetic strategies are needed to prepare the high MW block copolymers required, which combined with a greater understanding of the kinetics of self-assembly, will allow for these photonic materials to be produced industrially. One such opportunity for synthetic innovation is the ubiquitous use of norbornene as the backbone for BBCPs. While this has allowed for direct access to a wide range of macromonomers that can be readily converted via ROMP to BBCPs, the synthesis can be laborious and the polymerization necessitates the use of expensive metathesis catalysts, e.g., Grubbs catalysts. To move beyond a laboratory-scale endeavor it will be necessary for the community to develop substitute backbones that maintain efficient polymerization while offering a lower production cost. Alternatively, instead of covalently-bonded polymers, supramolecular copolymers could be explored as potential candidates as they offer flexible, modular design, and rapid polymer synthesis.[181–190] Finally, other factors (long-term stability, solvent compatibility, surface wetting etc.) of the self-assembled photonic materials need to be benchmarked if they are to displace existing technologies in the market, such as inorganic mica in effect pigments.

Beyond use as simple colorants, the incorporation of BCP-based photonic materials within smart devices, sensors, or displays has been strongly promoted within the literature. As such, studies to assess the viability of functional photonic BCP materials in these applications are required to identify the current challenges in successfully translating the technology. So far, the main limitation that hinders their full commercial potential remains synthetic diversity. New BCP compositions are rarely reported with, for example, almost all linear block copolymers comprising at least one block based on polystyrene and prepared via anionic polymerization of vinyl monomers.

This repeated use of the same monomers and polymerization routes has led to a lack of diversity in terms of chemical functionality, which limits the range of responsive materials that can be developed for, e.g., colorimetric sensors. With a more diverse pool of monomers, greater creativity and flexibility could be achieved in terms of polymer design with optimizations performed in silico. Furthermore, to ensure the long-term durability of these smart devices, non-volatile systems should be designed to replace the volatile solvents often used to achieve tunability and responsivity.

Finally, as awareness over the impact and accumulation of microplastics within the natural environment continues to grow, it is important for the community to consider the complete lifetime of BCP-based photonic materials. The current polymer systems used to produce BCPs are typically highly synthetic and as such degrade slowly, if at all. Therefore, it is imperative for the field to incorporate concepts of biocompatibility and/or biodegradability at the point of polymer conception, and to consider green chemical synthesis methods when preparing the polymers and selecting suitable solvents for self-assembly. In the short-term this could be achieved by, for example, incorporating degradable elements and biocompatible side chains onto the norbornene macromonomers favored within the BBCP community. However, in the long-term, this concern should drive the community to explore how to achieve high-performing photonic BCP-based materials exclusively from sustainable biopolymers (polylactic acid, polycaprolactone, polysaccharides, polypeptides, etc.). This approach will not only stimulate innovation in terms of polymer chemistry, but also finally achieve the goal of sustainable photonic materials.

Acknowledgements

This work was supported by the European Research Council [ERC-2014-STG H2020 639088; ERC-2017-POC 790518], the Biotechnology and Biological Science Research Council [BBSRC David Phillips Fellowship BB/K014617/1], the Engineering and Physical Sciences Research Council [EPSRC EP/N016920/1; EP/R511675/1], the Royal Society [IE160420], a CSC Cambridge Scholarship, a Croucher Cambridge International Scholarship and the Winton Program for the Physics of Sustainability. The authors thank Johannes Haataja for suggesting the visualization software for co-author collaboration network analysis, and Lukas Schertel for helpful discussions. This article is part of the *Advanced Optical Materials* Hall of Fame article series, which recognizes the excellent contributions of leading researchers to the field of optical materials science.

Conflict of Interest

The authors declare no conflict of interest.

Keywords

block copolymers, confinement, photonic crystals, photonic glasses, self-assembly

Received: March 12, 2021
Revised: June 21, 2021
Published online:

[1] R. Verduzco, X. Li, S. L. Pesek, G. E. Stein, *Chem. Soc. Rev.* **2015**, *44*, 2405.
[2] Y. Mai, A. Eisenberg, *Chem. Soc. Rev.* **2012**, *41*, 5969.
[3] C. Yi, Y. Yang, B. Liu, J. He, Z. Nie, *Chem. Soc. Rev.* **2020**, *49*, 465.
[4] Z. L. Tyrrell, Y. Shen, M. Radosz, *Prog. Polym. Sci.* **2010**, *35*, 1128.
[5] M. Stefik, S. Guldin, S. Vignolini, U. Wiesner, U. Steiner, *Chem. Soc. Rev.* **2015**, *44*, 5076.
[6] A. L. Liberman-Martin, C. K. Chu, R. H. Grubbs, *Macromol. Rapid. Commun.* **2017**, *38*, 1700058.
[7] E. Kim, S. Y. Kim, G. Jo, S. Kim, M. J. Park, *ACS Appl. Mater. Interfaces* **2012**, *4*, 5179.
[8] Q. Wang, K. H. Gu, Z. Y. Zhang, P. P. Hou, Z. H. Shen, X. H. Fan, *Polymer* **2018**, *156*, 169.
[9] C. Lu, M. W. Urban, *ACS Macro Lett.* **2015**, *4*, 1317.
[10] M. Poutanen, G. Guidetti, T. I. Gröschel, O. V. Borisov, S. Vignolini, O. Ikkala, A. H. Gröschel, *ACS Nano* **2018**, *12*, 3149.
[11] L. Han, D. Xu, Y. Liu, T. Ohsuna, Y. Yao, C. Jiang, Y. Mai, Y. Cao, Y. Duan, S. Che, *Chem. Mater.* **2014**, *26*, 7020.
[12] A. M. Urbas, M. Maldovan, P. DeRege, E. L. Thomas, *Adv. Mater.* **2002**, *14*, 1850.
[13] F. Yu, Q. Zhang, R. P. Thedford, A. Singer, D. M. Smilgies, M. O. Thompson, U. B. Wiesner, *ACS Nano* **2020**, *14*, 11273.
[14] Y. La, J. Song, M. G. Jeong, A. Cho, S.-M. Jin, E. Lee, K. T. Kim, *Nat. Commun.* **2018**, *9*, 5327.
[15] C. S. Wu, P. Y. Tsai, T. Y. Wang, E. L. Lin, Y. C. Huang, Y. W. Chiang, *Anal. Chem.* **2018**, *90*, 4847.
[16] Q. Xiang, Y. W. Luo, *Polymer* **2016**, *106*, 285.
[17] D. Ndaya, R. Bosire, R. M. Kasi, *ACS Appl. Polym. Mater.* **2020**, *2*, 5511.
[18] M. B. Runge, N. B. Bowden, *J. Am. Chem. Soc.* **2007**, *129*, 10551.
[19] Y. F. Yue, J. P. Gong, *J. Photochem. Photobiol., C* **2015**, *23*, 45.
[20] P. Lova, G. Manfredi, D. Comoretto, *Adv. Opt. Mater.* **2018**, *6*, 1800730.
[21] Y. Kang, J. Hyon, C. Seo, C. Bathula, in *Photonic Materials for Sensing, Biosensing and Display Devices*, Vol. *229*, (Eds: M. J. Serpe, Y. Kang, Q. M. Zhang), Springer, New York **2016**, p. 79.
[22] S. Kinoshita, S. Yoshioka, J. Miyazaki, *Rep. Prog. Phys.* **2008**, *71*, 076401.
[23] E. S. A. Goerlitzer, R. N. K. Taylor, N. Vogel, *Adv. Mater.* **2018**, *30*, 1706654.
[24] Y. Fu, C. A. Tippets, E. U. Donev, R. Lopez, *Wiley Interdiscip. Rev.: Nanomed. Nanobiotechnol.* **2016**, *8*, 758.
[25] Y. Fink, A. M. Urbas, M. G. Bawendi, J. D. Joannopoulos, E. L. Thomas, *J. Lightwave Technol.* **1999**, *17*, 1963.
[26] M. Bockstaller, R. Kolb, E. L. Thomas, *Adv. Mater.* **2001**, *13*, 1783.
[27] M. R. Bockstaller, Y. Lapetnikov, S. Margel, E. L. Thomas, *J. Am. Chem. Soc.* **2003**, *125*, 5276.
[28] M. R. Bockstaller, E. L. Thomas, *J. Phys. Chem. B* **2003**, *107*, 10017.
[29] J. Yoon, W. Lee, E. L. Thomas, *Nano Lett.* **2006**, *6*, 2211.
[30] Y. W. Chiang, C. Y. Chou, C. S. Wu, E. L. Lin, J. Yoon, E. L. Thomas, *Macromolecules* **2015**, *48*, 4004.
[31] S. H. Kim, K. S. Kim, K. Char, S. I. Yoo, B. H. Sohn, *Nanoscale* **2016**, *8*, 10823.
[32] J. Yoon, R. T. Mathers, G. W. Coates, E. L. Thomas, *Macromolecules* **2006**, *39*, 1913.
[33] P. D. Hustad, G. R. Marchand, E. I. Garcia-Meitin, P. L. Roberts, J. D. Weinhold, *Macromolecules* **2009**, *42*, 3788.
[34] J. K. D. Mapas, T. Thomay, A. N. Cartwright, J. Ilavsky, J. Rzayev, *Macromolecules* **2016**, *49*, 3733.
[35] M. Appold, E. Grune, H. Frey, M. Gallei, *ACS Appl. Mater. Interfaces* **2018**, *10*, 18202.
[36] N. J. van Eck, L. Waltman, *Scientometrics* **2010**, *84*, 523.
[37] N. J. van Eck, L. Waltman, in *Measuring Scholarly Impact: Methods and Practice*, (Eds: Y. Ding, R. Rousseau, D. Wolfram), Springer International Publishing, Cham, Switzerland **2014**, p. 285.

[38] Y. Kang, J. J. Walish, T. Gorishnyy, E. L. Thomas, *Nat. Mater.* **2007**, *6*, 957.
[39] E. Kim, C. Kang, H. Baek, K. Hwang, D. Kwak, E. Lee, Y. Kang, E. L. Thomas, *Adv. Funct. Mater.* **2010**, *20*, 1728.
[40] Y. B. Baek, S. H. Choi, D. M. Shin, *J. Nanosci. Nanotechnol.* **2015**, *15*, 1624.
[41] H. Xia, J. Zhao, C. Meng, Y. Wu, Y. Lu, J. Wang, Y. Song, L. Jiang, G. Zhang, *Soft Matter* **2011**, *7*, 4156.
[42] Y. Lu, H. Xia, G. Zhang, C. Wu, *J. Mater. Chem.* **2009**, *19*, 5952.
[43] J. J. Walish, Y. Kang, R. A. Mickiewicz, E. L. Thomas, *Adv. Mater.* **2009**, *21*, 3078.
[44] K. Hwang, D. Kwak, C. Kang, D. Kim, Y. Ahn, Y. Kang, *Angew. Chem., Int. Ed.* **2011**, *50*, 6311.
[45] Y. Lu, C. Meng, H. Xia, G. Zhang, C. Wu, *J. Mater. Chem. C* **2013**, *1*, 6107.
[46] Y. B. Baek, S. H. Choi, D. M. Shin, *Mol. Cryst. Liq. Cryst.* **2014**, *600*, 9.
[47] S. N. Lee, Y. Bin Baek, D. M. Shin, *J. Nanosci. Nanotechnol.* **2014**, *14*, 6053.
[48] T. J. Park, S. K. Hwang, S. Park, S. H. Cho, T. H. Park, B. Jeong, H. S. Kang, D. Y. Ryu, J. Huh, E. L. Thomas, C. Park, *ACS Nano* **2015**, *9*, 12158.
[49] Y. Kang, *Bull. Korean Chem. Soc.* **2008**, *29*, 2329.
[50] S. E. Shin, S. Y. Kim, D. M. Shin, *J. Nanosci. Nanotechnol.* **2011**, *11*, 4275.
[51] Y. Ahn, E. Kim, J. Hyon, C. Kang, Y. Kang, *Adv. Mater.* **2012**, *24*, OP127.
[52] H. S. Lim, J.-H. Lee, J. J. Walish, E. L. Thomas, *ACS Nano* **2012**, *6*, 8933.
[53] O. B. Ayyub, M. B. Ibrahim, P. Kofinas, *Polymer* **2014**, *55*, 6227.
[54] S. E. Shin, S. Y. Kim, D. M. Shin, *Mol. Cryst. Liq. Cryst.* **2010**, *520*, 122/[398].
[55] S. W. Lee, J. Shin, J. Shin, C. Shim, D. M. Shin, *Mol. Cryst. Liq. Cryst.* **2011**, *539*, 96.
[56] Y. Kang, *Bull. Korean Chem. Soc.* **2012**, *33*, 2847.
[57] Y. Kang, *Macromol. Res.* **2012**, *20*, 1223.
[58] Y. Jang, J. Chung, S. Lee, H. Lim, H. Baek, Y. Kang, *Polym. Bull.* **2013**, *70*, 593.
[59] Y. Fan, J. J. Walish, S. Tang, B. D. Olsen, E. L. Thomas, *Macromolecules* **2014**, *47*, 1130.
[60] A. Noro, Y. Tomita, Y. Shinohara, Y. Sageshima, J. J. Walish, Y. Matsushita, E. L. Thomas, *Macromolecules* **2014**, *47*, 4103.
[61] J. Y. Lim, S. Y. Park, S. W. Lee, J. H. Yun, S. H. Choi, D. M. Shin, *J. Nanosci. Nanotechnol.* **2016**, *16*, 8407.
[62] A. Noro, Y. Tomita, Y. Matsushita, E. L. Thomas, *Macromolecules* **2016**, *49*, 8971.
[63] J. Y. Lim, J. B. Ju, D. M. Shin, *Mol. Cryst. Liq. Cryst.* **2017**, *650*, 110.
[64] J. Y. Lim, D. M. Shin, *Mol. Cryst. Liq. Cryst.* **2017**, *654*, 214.
[65] Y. N. Oh, S. Y. Lee, D. M. Shin, *Mol. Cryst. Liq. Cryst.* **2017**, *659*, 59.
[66] Y. N. Oh, S. Y. Lee, D. M. Shin, *Mol. Cryst. Liq. Cryst.* **2017**, *653*, 17.
[67] E. L. Lin, W. L. Hsu, Y. W. Chiang, *ACS Nano* **2018**, *12*, 485.
[68] E. P. Chan, J. J. Walish, E. L. Thomas, C. M. Stafford, *Adv. Mater.* **2011**, *23*, 4702.
[69] J. J. Walish, Y. Fan, A. Centrone, E. L. Thomas, *Macromol. Rapid. Commun.* **2012**, *33*, 1504.
[70] C. Kang, E. Kim, H. Baek, K. Hwang, D. Kwak, Y. Kang, E. L. Thomas, *J. Am. Chem. Soc.* **2009**, *131*, 7538.
[71] O. B. Ayyub, J. W. Sekowski, T.-I. Yang, X. Zhang, R. M. Briber, P. Kofinas, *Biosens. Bioelectron.* **2011**, *28*, 349.
[72] O. B. Ayyub, M. B. Ibrahim, R. M. Briber, P. Kofinas, *Biosens. Bioelectron.* **2013**, *46*, 124.
[73] T. H. Park, S. Yu, S. H. Cho, H. S. Kang, Y. Kim, M. J. Kim, H. Eoh, C. Park, B. Jeong, S. W. Lee, D. Y. Ryu, J. Huh, C. Park, *NPG Asia Mater.* **2018**, *10*, 328.
[74] E. Lee, J. Kim, J. Myung, Y. Kang, *Macromol. Res.* **2012**, *20*, 1219.
[75] Y. Fan, S. Tang, E. L. Thomas, B. D. Olsen, *ACS Nano* **2014**, *8*, 11467.
[76] H. S. Kang, J. Lee, S. M. Cho, T. H. Park, M. J. Kim, C. Park, S. W. Lee, K. L. Kim, D. Y. Ryu, J. Huh, E. L. Thomas, C. Park, *Adv. Mater.* **2017**, *29*, 1700084.
[77] H. Kosonen, S. Valkama, J. Ruokolainen, M. Torkkeli, R. Serimaa, G. ten Brinke, O. Ikkala, *Eur. Phys. J. E* **2003**, *10*, 69.
[78] S. Valkama, H. Kosonen, J. Ruokolainen, T. Haatainen, M. Torkkeli, R. Serimaa, G. Ten Brinke, O. Ikkala, *Nat. Mater.* **2004**, *3*, 872.
[79] A. M. Urbas, E. L. Thomas, H. Kriegs, G. Fytas, R. S. Penciu, L. N. Economou, *Phys. Rev. Lett.* **2003**, *90*, 108302.
[80] W. M. Lee, J. S. Yoon, H. J. Lee, E. L. Thomas, *Macromolecules* **2007**, *40*, 6021.
[81] J. Yoon, W. Lee, E. L. Thomas, *Macromolecules* **2008**, *41*, 4582.
[82] A. J. Parnell, A. Pryke, O. O. Mykhaylyk, J. R. Howse, A. M. Adawi, N. J. Terrill, J. P. A. Fairclough, *Soft Matter* **2011**, *7*, 3721.
[83] A. J. Parnell, N. Tzokova, A. Pryke, J. R. Howse, O. O. Mykhaylyk, A. J. Ryan, P. Panine, J. P. A. Fairclough, *Phys. Chem. Chem. Phys.* **2011**, *13*, 3179.
[84] W. Lee, J. Yoon, E. L. Thomas, H. Lee, *Macromolecules* **2013**, *46*, 6528.
[85] Y. W. Chiang, J. J. Chang, C. Y. Chou, C. S. Wu, E. L. Lin, E. L. Thomas, *Adv. Opt. Mater.* **2015**, *3*, 1517.
[86] A. Matsushita, S. Okamoto, *Macromolecules* **2014**, *47*, 7169.
[87] A. Matsushita, S. Okamoto, *Polym. J.* **2015**, *47*, 385.
[88] A. Urbas, Y. Fink, E. L. Thomas, *Macromolecules* **1999**, *32*, 4748.
[89] A. Urbas, R. Sharp, Y. Fink, E. L. Thomas, M. Xenidou, L. J. Fetters, *Adv. Mater.* **2000**, *12*, 812.
[90] C. Osuji, C. Y. Chao, I. Bita, C. K. Ober, E. L. Thomas, *Adv. Funct. Mater.* **2002**, *12*, 753.
[91] R. Motokawa, T. Taniguchi, T. Kumada, Y. Iida, S. Aoyagi, Y. Sasaki, M. Kohri, K. Kishikawa, *Macromolecules* **2016**, *49*, 6041.
[92] K. Tsuchiya, S. Nagayasu, S. Okamoto, T. Hayakawa, T. Hihara, K. Yamamoto, I. Takumi, S. Hara, H. Hasegawa, S. Akasaka, N. Kosikawa, *Opt. Express* **2008**, *16*, 5362.
[93] T. Yamanaka, S. Hara, T. Hirohata, *Opt. Express* **2011**, *19*, 24583.
[94] Y. C. Huang, Y. Zheng, J. Pribyl, B. C. Benicewicz, *J. Mater. Chem. C* **2017**, *5*, 9873.
[95] W. Cao, S. Xia, M. Appold, N. Saxena, L. Bießmann, S. Grott, N. Li, M. Gallei, S. Bernstorff, P. Müller-Buschbaum, *Sci. Rep.* **2019**, *9*, 18269.
[96] H. Cui, Z. Chen, S. Zhong, K. L. Wooley, D. J. Pochan, *Science* **2007**, *317*, 647.
[97] J. Rzayev, *Macromolecules* **2009**, *42*, 2135.
[98] Y. Xia, B. D. Olsen, J. A. Kornfield, R. H. Grubbs, *J. Am. Chem. Soc.* **2009**, *131*, 18525.
[99] V. A. Piunova, G. M. Miyake, C. S. Daeffler, R. A. Weitekamp, R. H. Grubbs, *J. Am. Chem. Soc.* **2013**, *135*, 15609.
[100] A. Aluculesei, A. Pipertzis, V. A. Piunova, G. M. Miyake, G. Floudas, G. Fytas, R. H. Grubbs, *Macromolecules* **2015**, *48*, 4142.
[101] B. M. Boyle, T. A. French, R. M. Pearson, B. G. McCarthy, G. M. Miyake, *ACS Nano* **2017**, *11*, 3052.
[102] G. M. Miyake, R. A. Weitekamp, V. A. Piunova, R. H. Grubbs, *J. Am. Chem. Soc.* **2012**, *134*, 14249.
[103] G. M. Miyake, V. A. Piunova, R. A. Weitekamp, R. H. Grubbs, *Angew. Chem., Int. Ed.* **2012**, *51*, 11246.
[104] B. R. Sveinbjoernsson, R. A. Weitekamp, G. M. Miyake, Y. Xia, H. A. Atwater, R. H. Grubbs, *Proc. Natl. Acad. Sci. USA* **2012**, *109*, 14332.
[105] R. J. Macfarlane, B. Kim, B. Lee, R. A. Weitekamp, C. M. Bates, S. F. Lee, A. B. Chang, K. T. Delaney, G. H. Fredrickson, H. A. Atwater, R. H. Grubbs, *J. Am. Chem. Soc.* **2014**, *136*, 17374.
[106] Y. P. Qiao, Y. D. Zhao, X. Y. Yuan, Y. H. Zhao, L. X. Ren, *J. Mater. Sci.* **2018**, *53*, 16160.

[107] D. P. Song, C. Li, N. S. Colella, X. M. Lu, J. H. Lee, J. J. Watkins, *Adv. Opt. Mater.* **2015**, *3*, 1169.
[108] D. P. Song, C. Li, W. H. Li, J. J. Watkins, *ACS Nano* **2016**, *10*, 1216.
[109] D. P. Song, G. Jacucci, F. Dundar, A. Naik, H. F. Fei, S. Vignolini, J. J. Watkins, *Macromolecules* **2018**, *51*, 2395.
[110] C. G. Chae, Y. G. Yu, M. J. Kim, R. H. Grubbs, J. S. Lee, *Macromolecules* **2018**, *51*, 3458.
[111] D. P. Song, T. H. H. Zhao, G. Guidetti, S. Vignolini, R. M. Parker, *ACS Nano* **2019**, *13*, 1764.
[112] I. H. Lee, D. M. Shin, *Mol. Cryst. Liq. Cryst.* **2019**, *685*, 64.
[113] H. S. Kang, S. W. Han, C. Park, S. W. Lee, H. Eoh, J. Baek, D. G. Shin, T. H. Park, J. Huh, H. Lee, D. E. Kim, D. Ryu, E. L. Thomas, W. G. Koh, C. Park, *Sci. Adv.* **2020**, *6*, eabb5769.
[114] T. H. Park, H. Eoh, Y. Jung, G.-W. Lee, C. E. Lee, H. S. Kang, J. Lee, K.-B. Kim, D. Y. Ryu, S. Yu, C. Park, *Adv. Funct. Mater.* **2021**, *31*, 2008548.
[115] H. Eoh, H. S. Kang, M. J. Kim, M. Koo, T. H. Park, Y. Kim, H. Lim, D. Y. Ryu, E. Kim, J. Huh, Y. Kang, C. Park, *Adv. Funct. Mater.* **2019**, *29*, 1904055.
[116] R. M. Zhang, Z. Qiang, M. Z. Wang, *Adv. Funct. Mater.* **2021**, *31*, 2005819.
[117] A. Subramanian, N. Tiwale, G. Doerk, K. Kisslinger, C. Y. Nam, *ACS Appl. Mater. Interfaces* **2020**, *12*, 1444.
[118] M. Plank, F. Hartmann, B. Kuttich, T. Kraus, M. Gallei, *Eur. Polym. J.* **2020**, 110059.
[119] Y. F. Xu, R. J. Hickey, *Macromolecules* **2020**, *53*, 5711.
[120] M. J. Kim, Y. G. Yu, C. G. Chae, H. B. Seo, I. G. Bak, Y. Mallela, J. S. Lee, *Macromolecules* **2019**, *52*, 103.
[121] S. J. Dalsin, T. G. Rions-Maehren, M. D. Beam, F. S. Bates, M. A. Hillmyer, M. W. Matsen, *ACS Nano* **2015**, *9*, 12233.
[122] Y. G. Yu, C. G. Chae, M. J. Kim, H. B. Seo, R. H. Grubbs, J. S. Lee, *Macromolecules* **2018**, *51*, 447.
[123] Y. G. Yu, C. Seo, C. G. Chae, H. B. Seo, M. J. Kim, Y. Kang, J. S. Lee, *Macromolecules* **2019**, *52*, 4349.
[124] H. B. Seo, Y. G. Yu, C. G. Chae, M. J. Kim, J. S. Lee, *Polymer* **2019**, *177*, 241.
[125] T. T. Guo, X. L. Yu, Y. H. Zhao, X. Y. Yuan, J. Y. Li, L. X. Ren, *Macromolecules* **2020**, *53*, 3602.
[126] T. Z. Zhang, J. X. Yang, X. L. Yu, Y. S. Li, X. Y. Yuan, Y. H. Zhao, D. Lyu, Y. F. Men, K. Zhang, L. X. Ren, *Polym. Chem.* **2019**, *10*, 1519.
[127] Y. D. Zhao, T. T. Guo, J. X. Yang, Y. S. Li, X. Y. Yuan, Y. H. Zhao, L. X. Ren, *React. Funct. Polym.* **2019**, *139*, 162.
[128] T. T. Guo, Y. Wang, Y. P. Qiao, X. Y. Yuan, Y. H. Zhao, L. X. Ren, *Polymer* **2020**, *194*, 122389.
[129] B. M. Boyle, J. L. Collins, T. E. Mensch, M. D. Ryan, B. S. Newell, G. M. Miyake, *Polym. Chem.* **2020**, *11*, 7147.
[130] M. A. Wade, D. Walsh, J. C. W. Lee, E. Kelley, K. Weigandt, D. Guironnet, S. A. Rogers, *Soft Matter* **2020**, *16*, 4919.
[131] B. B. Patel, D. J. Walsh, D. H. Kim, J. Kwok, B. Lee, D. Guironnet, Y. Diao, *Sci. Adv.* **2020**, *6*, eaaz7202.
[132] M. C. Orilall, U. Wiesner, *Chem. Soc. Rev.* **2011**, *40*, 520.
[133] S. Ji, L. Wan, C.-C. Liu, P. F. Nealey, *Prog. Polym. Sci.* **2016**, *54-55*, 76.
[134] W. Li, M. Müller, *Prog. Polym. Sci.* **2016**, *54-55*, 47.
[135] Z. Li, M. Tang, S. Liang, M. Zhang, G. M. Biesold, Y. He, S.-M. Hao, W. Choi, Y. Liu, J. Peng, Z. Lin, *Prog. Polym. Sci.* **2021**, *116*, 101387.
[136] F. S. Bates, G. H. Fredrickson, *Phys. Today* **1999**, *52*, 32.
[137] W.-N. He, J.-T. Xu, *Prog. Polym. Sci.* **2012**, *37*, 1350.
[138] Y. Deng, J. Wei, Z. Sun, D. Zhao, *Chem. Soc. Rev.* **2013**, *42*, 4054.
[139] H. Feng, X. Lu, W. Wang, N.-G. Kang, J. W. Mays, *Polymers* **2017**, *9*, 494.
[140] A. Blanazs, S. P. Armes, A. J. Ryan, *Macromol. Rapid. Commun.* **2009**, *30*, 267.
[141] V. Castelletto, I. W. Hamley, *Curr. Opin. Solid State Mater. Sci.* **2004**, *8*, 426.
[142] T. H. Zhao, G. Jacucci, X. Chen, D.-P. Song, S. Vignolini, R. M. Parker, *Adv. Mater.* **2020**, *32*, 2002681.
[143] C. Sinturel, F. S. Bates, M. A. Hillmyer, *ACS Macro Lett.* **2015**, *4*, 1044.
[144] C. X. Wang, X. M. Li, H. Deng, *ACS Macro Lett.* **2019**, *8*, 368.
[145] D. F. Sunday, M. J. Maher, A. F. Hannon, C. D. Liman, S. Tein, G. Blachut, Y. Asano, C. J. Ellison, C. G. Willson, R. J. Kline, *Macromolecules* **2018**, *51*, 173.
[146] W. Zhang, M. Huang, S. a. Abdullatif, M. Chen, Y. Shao-Horn, J. A. Johnson, *Macromolecules* **2018**, *51*, 6757.
[147] A. E. Levi, J. Lequieu, J. D. Horne, M. W. Bates, J. M. Ren, K. T. Delaney, G. H. Fredrickson, C. M. Bates, *Macromolecules* **2019**, *52*, 1794.
[148] M.-J. Kim, Y.-G. Yu, C.-G. Chae, H.-B. Seo, I.-G. Bak, Y. L. N. K. Mallela, J.-S. Lee, *Macromolecules* **2019**, *52*, 103.
[149] N. Yan, Y. T. Zhu, W. Jiang, *Chem. Commun.* **2018**, *54*, 13183.
[150] K. H. Ku, J. M. Shin, H. Yun, G. R. Yi, S. G. Jang, B. J. Kim, *Adv. Funct. Mater.* **2018**, *28*, 1802961.
[151] H. Yabu, T. Higuchi, H. Jinnai, *Soft Matter* **2014**, *10*, 2919.
[152] R. Deng, J. Xu, G.-R. Yi, J. W. Kim, J. Zhu, *Adv. Funct. Mater.* **2021**, *31*, 2008169.
[153] C. K. Wong, X. Qiang, A. H. E. Müller, A. H. Gröschel, *Prog. Polym. Sci.* **2020**, *102*, 101211.
[154] A. H. Groschel, A. H. E. Muller, *Nanoscale* **2015**, *7*, 11841.
[155] Y. Zhao, L. Shang, Y. Cheng, Z. Gu, *Acc. Chem. Res.* **2014**, *47*, 3632.
[156] J. Y. Wang, J. T. Zhu, *Eur. Polym. J.* **2013**, *49*, 3420.
[157] T. Brugarolas, F. Tu, D. Lee, *Soft Matter* **2013**, *9*, 9046.
[158] F. Li, D. P. Josephson, A. Stein, *Angew. Chem., Int. Ed.* **2011**, *50*, 360.
[159] N. Vogel, S. Utech, G. T. England, T. Shirman, K. R. Phillips, N. Koay, I. B. Burgess, M. Kolle, D. A. Weitz, J. Aizenberg, *Proc. Natl. Acad. Sci. USA* **2015**, *112*, 10845.
[160] A. G. Dumanli, T. Savin, *Chem. Soc. Rev.* **2016**, *45*, 6698.
[161] C. Fenzl, T. Hirsch, O. S. Wolfbeis, *Angew. Chem., Int. Ed.* **2014**, *53*, 3318.
[162] Y. Yang, H. Kim, J. Xu, M.-S. Hwang, D. Tian, K. Wang, L. Zhang, Y. Liao, H.-G. Park, G.-R. Yi, X. Xie, J. Zhu, *Adv. Mater.* **2018**, *30*, 1707344.
[163] Y. Yang, Y. Chen, Z. Hou, F. Li, M. Xu, Y. Liu, D. Tian, L. Zhang, J. Xu, J. Zhu, *ACS Nano* **2020**, *14*, 16057.
[164] Y. Yang, T. H. Kang, K. Wang, M. Ren, S. B. Chen, B. J. Xiong, J. P. Xu, L. B. Zhang, G. R. Yi, J. T. Zhu, *Small* **2020**, *16*, 2001315.
[165] Y. Yang, H. Kim, J. P. Xu, M. S. Hwang, D. Tian, K. Wang, L. B. Zhang, Y. G. Liao, H. G. Park, G. R. Yi, X. L. Xie, J. T. Zhu, *Adv. Mater.* **2018**, *30*, 1707344.
[166] Q. He, K. H. Ku, H. Vijayamohanan, B. J. Kim, T. M. Swager, *J. Am. Chem. Soc.* **2020**, *142*, 10424.
[167] E. J. Kim, J. J. Shin, T. Do, G. S. Lee, J. Park, V. Thapar, J. Choi, J. Bang, G.-R. Yi, S.-M. Hur, J. G. Kim, B. J. Kim, *ACS Nano* **2021**, *15*, 5513.
[168] G. Jacucci, S. Vignolini, L. Schertel, *Proc. Natl. Acad. Sci. USA* **2020**, *117*, 23345.
[169] X. Chen, X. Yang, D.-P. Song, Y.-F. Men, Y. Li, *Macromolecules* **2021**, *54*, 3668.
[170] Y.-L. Li, X. Chen, H.-K. Geng, Y. Dong, B. Wang, Z. Ma, L. Pan, G.-Q. Ma, D.-P. Song, Y.-S. Li, *Angew. Chem., Int. Ed.* **2020**, *60*, 3647.
[171] Q.-J. Liu, Y. Li, J.-C. Xu, H.-F. Lu, Y. Li, D.-P. Song, *ACS Nano* **2021**, *15*, 5534.
[172] J. Ge, Y. Yin, *Angew. Chem., Int. Ed.* **2011**, *50*, 1492.
[173] E. Hecht, *Optics, Global Edition*, Pearson Education Limited, London **2016**.

[174] L. Maiwald, S. Lang, D. Jalas, H. Renner, A. Y. Petrov, M. Eich, *Opt. Express* **2018**, *26*, 11352.
[175] G. Shang, L. Maiwald, H. Renner, D. Jalas, M. Dosta, S. Heinrich, A. Petrov, M. Eich, *Sci. Rep.* **2018**, *8*, 7804.
[176] F. Liu, B. Q. Dong, X. H. Liu, Y. M. Zheng, J. Zi, *Opt. Express* **2009**, *17*, 16183.
[177] S. Magkiriadou, J.-G. Park, Y.-S. Kim, V. N. Manoharan, *Phys. Rev. E* **2014**, *90*, 062302.
[178] G. H. Lee, J. Y. Sim, S.-H. Kim, *ACS Appl. Mater. Interfaces* **2016**, *8*, 12473.
[179] C. L. C. Chan, M. M. Bay, G. Jacucci, R. Vadrucci, C. A. Williams, G. T. van de Kerkhof, R. M. Parker, K. Vynck, B. Frka-Petesic, S. Vignolini, *Adv. Mater.* **2019**, *31*, 1905151.
[180] L. Schertel, L. Siedentop, J.-M. Meijer, P. Keim, C. M. Aegerter, G. J. Aubry, G. Maret, *Adv. Opt. Mater.* **2019**, *7*, 1900442.
[181] M. Wehner, F. Würthner, *Nat. Rev. Chem.* **2020**, *4*, 38.
[182] B. Qin, Z. Yin, X. Tang, S. Zhang, Y. Wu, J.-F. Xu, X. Zhang, *Prog. Polym. Sci.* **2020**, *100*, 101167.
[183] Z. Huang, B. Qin, L. Chen, J.-F. Xu, C. F. J. Faul, X. Zhang, *Macromol. Rapid. Commun.* **2017**, *38*, 1700312.
[184] A. Sorrenti, J. Leira-Iglesias, A. J. Markvoort, T. F. A. de Greef, T. M. Hermans, *Chem. Soc. Rev.* **2017**, *46*, 5476.
[185] L. Yang, X. Tan, Z. Wang, X. Zhang, *Chem. Rev.* **2015**, *115*, 7196.
[186] S.-L. Li, T. Xiao, C. Lin, L. Wang, *Chem. Soc. Rev.* **2012**, *41*, 5950.
[187] F. Huang, O. A. Scherman, *Chem. Soc. Rev.* **2012**, *41*, 5879.
[188] T. Aida, E. W. Meijer, S. I. Stupp, *Science* **2012**, *335*, 813.
[189] T. F. A. De Greef, M. M. J. Smulders, M. Wolffs, A. P. H. J. Schenning, R. P. Sijbesma, E. W. Meijer, *Chem. Rev.* **2009**, *109*, 5687.
[190] T. F. A. de Greef, E. W. Meijer, *Nature* **2008**, *453*, 171.

Zhen Wang received his B.Sc. and M.Sc. in chemistry from Renmin University of China. Currently, he is pursuing a Ph.D. under the supervision of Prof. Silvia Vignolini, in the Bio-inspired Photonics group within the Yusuf Hamied Department of Chemistry at the University of Cambridge. His research interests focus on the synthesis of bio-based brush block copolymers and their applications in structural colors.

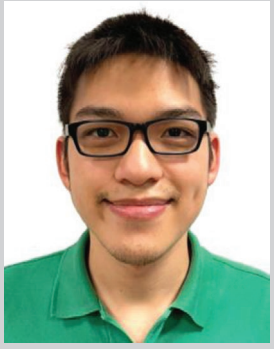

Chun Lam Clement Chan graduated in 2017 with a degree in natural sciences (M.Sc.) from the University of Cambridge, where he is currently pursuing a Ph.D. under the supervision of Prof. Silvia Vignolini at the Yusuf Hamied Department of Chemistry. His work focuses on developing solid-state photonic structures based on cellulosic polymers and other biocompatible polymeric systems.

Tianheng H. Zhao graduated from Monash University (Australia) with a degree in Materials Science and Engineering (B.Eng.) in 2014. He then continued his studies at the University of Cambridge for his master and Ph.D. degrees. He has recently completed his Ph.D. degree under the supervision of Prof. Silvia Vignolini, in the Bio-inspired Photonics group at the Yusuf Hamied Department of Chemistry, University of Cambridge. His research centers around the geometrically confined self-assembly process of photonic building blocks such as cellulose nanocrystals and bottlebrush block copolymers.

Richard M. Parker graduated from the University of Southampton (UK) with a degree in chemistry (M.Chem.) in 2007, followed by the award of a Ph.D. in chemistry with optoelectronics in 2011. This was followed by a fellowship that combined the fields of photonic sensors, fiber optics, and supramolecular chemistry. In 2012, he moved to the University of Cambridge (UK), where he is currently a senior postdoctoral research associate. His research exploits self-assembly processes within ink-jet or microfluidic droplets to prepare novel material architectures; with interests ranging from supramolecular microcapsules and gels, to bio-inspired photonic microparticles and structurally colored films.

Silvia Vignolini studied physics at the University of Florence, Italy. In 2009, she was awarded a Ph.D. in solid-state physics at the University of Florence. In 2010, she moved to Cambridge as a postdoctoral research associate working in the Cavendish Laboratory and the Plant Science Department. She started her independent research by becoming a BBSRC David Philips Fellow in 2013. She is currently a Professor at the University of Cambridge in Chemistry and Bio-inspired materials.